water

MDPI

Article

70 Years of Shoreline Changes in Southern Sardinia (Italy): Retreat and Accretion on 79 Mediterranean Microtidal Beaches

Antonio Usai [1], Daniele Trogu [1,*], Marco Porta [1], Sandro Demuro [1] and Simone Simeone [2]

[1] Department of Chemical and Geological Sciences, Coastal and Marine Geomorphology Group (CMGG), University of Cagliari, 09042 Monserrato, Italy; antonio.usai@unica.it (A.U.); marcoporta@unica.it (M.P.); demuros@unica.it (S.D.)
[2] CNR-IAS, Institute for the Study of Anthropic Impacts and Sustainability in Marine Environment, National Research Council, 09170 Oristano, Italy; simone.simeone@cnr.it
* Correspondence: d.trogu@unica.it; Tel.: +39-070-6757778

Abstract

Coastal erosion and shoreline change represent major challenges for the sustainable management of coastal environments, with implications for infrastructure, ecosystems, biodiversity, and the socio-economic well-being of coastal communities. This study investigates the shoreline evolution of 79 Mediterranean microtidal beaches located along the southern coast of Sardinia Island (Italy), using the Digital Shoreline Analysis System (DSAS). Shorelines were manually digitised from high-resolution aerial orthophotos made available through the WMS service of the Autonomous Region of Sardinia, covering the period 1954–2022. Shoreline changes were assessed through five statistical indicators: Shoreline Change Envelope (SCE), Net Shoreline Movement (NSM), End Point Rate (EPR), Weighted Linear Regression (WLR), and Linear Regression Rate (LRR). The results highlight marked spatial and temporal variability in shoreline retreat and accretion, revealing patterns that link shoreline dynamics to the degree of anthropisation or naturalness of each beach. In fact, coastal areas characterised by local anthropogenic factors showed higher rates of shoreline retreat and/or accretion, while natural beaches showed greater stability and resilience in the long term. The outcomes of this analysis provide valuable insights into local coastal dynamics and represent a critical knowledge base for developing targeted adaptation strategies, supporting spatial planning, and reducing coastal risks under future climate change scenarios.

Keywords: DSAS; coastal management; shoreline evolution; Mediterranean

Academic Editors: Nicolas Lecoq and Nizar Abcha

Received: 23 July 2025
Revised: 16 August 2025
Accepted: 21 August 2025
Published: 23 August 2025

Citation: Usai, A.; Trogu, D.; Porta, M.; Demuro, S.; Simeone, S. 70 Years of Shoreline Changes in Southern Sardinia (Italy): Retreat and Accretion on 79 Mediterranean Microtidal Beaches. *Water* **2025**, *17*, 2517. https://doi.org/10.3390/w17172517

1. Introduction

Coastal environments are dynamic systems, constantly evolving due to the interaction between natural and anthropogenic factors that drive erosion and sedimentation processes [1]. Coastal erosion is a phenomenon that is observed around the world. It is predicted to accelerate under the combined influence of several factors, including sea level rise driven by climate change, changes in wave climate, reduced fluvial sediment supply, and the impacts of coastal urbanisation. [2–4].

Recent studies have shown that the Mediterranean Sea is also experiencing the impacts of global climate change [5,6]. However, in semi-enclosed basins such as the Mediterranean Sea, projecting future trends in storm frequency and intensity remains challenging due to spatial heterogeneity and limited data coverage [7–11]. Tide-gauge networks and satellite altimetry show decadal sea-level increases ranging between approximately 2.5 and 3.6 mm

per year in the early 21st century, with significant regional variability owing to factors such as vertical land movements and subsidence [12–15]. These trends amplify both the frequency and intensity of storm-induced surges, especially in semi-enclosed basins (e.g., Adriatic, Aegean, Tunisian coasts), where beach flooding can occur due to the combined effects of tidal, meteorological and wave dynamic interactions [12].

The Mediterranean Sea is also distinguished by the presence of extensive meadows of *Posidonia oceanica*, a seagrass species endemic to the region, which constitutes one of the most significant coastal ecosystems. These meadows act as biodiversity hotspots, provide nursery habitats for numerous marine species, contribute to water quality through oxygen production, and play a crucial role in coastal protection by stabilising sediments and attenuating wave energy [16,17].

In microtidal environments, such as those of Mediterranean beaches, even small variations in hydrodynamic conditions and/or sediment budgets can produce significant shoreline changes [18,19]. This is particularly critical for embayed beaches (also known as pocket beaches; [20]), which function as quasi-closed sedimentary systems with limited connectivity to adjacent sandy systems and minimal fluvial or longshore sediment inputs. Being laterally bounded by rocky headlands [21,22], the morphodynamic equilibrium of embayed beaches relies on a delicate balance among wave energy, sediment availability, and local topography [23]. Moreover, their limited spatial extent and high tourist pressure further increase their vulnerability to erosion and habitat degradation.

Vulnerability assessment studies reveal that almost 50% of Mediterranean coastal systems, especially sandy, low-lying beaches, are highly susceptible to erosion, coastal flooding, and saltwater intrusion, with socio-economic factors contributing to further amplifying the risk [15,24,25]. In this context, there is an urgent need to implement adaptive and site-specific coastal management strategies based on robust and objective datasets to mitigate the impacts of sea level rise and reduce the vulnerability of Mediterranean coastal areas.

Human interventions have profoundly altered the morphology of the Mediterranean coast [26,27]. The construction of ports, tourist infrastructure, and urban settlements has disrupted natural sediment transport pathways, accelerating erosional processes in many areas [28,29]. In recent years, one of the most widespread anthropogenic practices observed throughout the study area is the removal of large volumes of *Posidonia oceanica* banquettes using heavy mechanical vehicles [30]. Banquettes, also known as seagrass berm, are natural sedimentary deposits composed of leaves, roots, and rhizomes of *Posidonia oceanica*, mixed with sand, that accumulate in the dry beach, at the upper limit of the wave action zone. [30]. Although this practice is primarily undertaken for aesthetic and recreational purposes, it may cause impacts such as compaction and removal of sand, alter the natural morphology of the beach, and significantly reduce the capacity of the coastal system to dissipate wave energy. Consequently, the beach's resilience to storm events is compromised and its vulnerability to shoreline retreat is increased [31–35]. Moreover, the implementation of beach nourishment is frequently utilised as a mitigation strategy [36,37]. In some cases, this has led to the modification of natural characteristics, and, at times, it has been observed to exacerbate shoreline retreat [38]. The effective management of the coast necessitates the integration of scientific shoreline monitoring, spatial-temporal analysis, and strategic planning in order to preserve the ecological integrity, as well as the socio-economic functions of beaches.

Recent advances in remote sensing technologies, GIS-based shoreline trend detection, and integrated coastal risk indices have significantly improved the development of robust, regionally calibrated frameworks for coastal risk assessment and long-term monitoring [39–41]. Within this context, the systematic reconstruction and analysis of historical

shoreline positions remains a fundamental approach for understanding coastal morphodynamics [42–46], identifying long-term retreat and accretion trends, and informing the design of evidence-based adaptation strategies. One of the most widely used tools for this purpose worldwide is the Digital Shoreline Analysis System (DSAS) [47], which has been extensively applied in diverse coastal settings to quantify shoreline change rates across multiple spatial and temporal scales [48–51]. However, despite the increasing availability of geospatial data and analytical tools, some Mediterranean coastal regions remain understudied, resulting in significant gaps in the literature. One such area is southern Sardinia, where coastal morphology is highly heterogeneous, ranging from natural dune-backed systems to heavily anthropised beaches.

This study aims to estimate the shoreline trends of 79 microtidal Mediterranean beaches along the southern coast of Sardinia Island (Italy) using the DSAS. By analysing aerial orthophotos from 1954 to 2022, long-term retreat and accretion rates have been quantified, as well as how these resulting patterns are related to both climate-driven forces and anthropogenic modifications. This approach provides a spatially explicit, data-driven basis for future beach management and conservation strategies in the context of accelerating environmental change.

2. Materials and Methods

2.1. Geographical Setting of the Study Area

The study area is located in Southern Sardinia (Italy, western Mediterranean Sea) along a coastal stretch of about 130 km, between Cape Teulada and Cape Carbonara (Figure 1). Along this coastline, both rocky and sandy shorelines can be found. A total of 79 microtidal beaches were analysed. These beaches vary greatly in terms of length and cross-shore extension: although many of them can be classified as embayed beaches with a high degree of embaymentisation [52], the studied coastline also includes beaches that are several kilometres long and have limited bay indentation [53]. They are mainly characterised by sandy sediments, with grain sizes ranging from fine to coarse. In some locations, particularly along the western coastline, pebble sediments are also present. The entire study area is characterised by the presence of *Posidonia oceanica* meadow, whose upper limit, varying among the different beaches, can be located at different distances from the shoreline [54] (Figure 1). This variability is influenced by several factors, including local hydrodynamic conditions, water turbidity, and, in some cases, the morphological characteristics of the seabed. In addition to their ecological function, these meadows may play a crucial role in the dissipation of wave energy and the offshore trapping of sediment, thus promoting beach stability and enhancing the coastal system's resilience to extreme events. [54]. Moreover, the studied coastal stretch exhibits spatial variability in coastal exposure and wave conditions [28,52,53,55,56].

Within the study area, the degree of human anthropisation along the coastline, as well as in the associated river catchments, exhibits significant spatial variability, closely related to the proximity of main urban centres. These consist of 26 artificial basins, including 15 dams, which could affect the supply of sediment in the study area [57]. Moreover, interventions to stabilise rocky cliffs bordering beaches, particularly those involving anchored mesh systems, may also affect the amount of sediment entering the coastal system by reducing the natural supply of sediment derived from erosion of the rock face [28]. Finally, one of the most common anthropogenic alterations affecting beach systems is the urbanisation of dune areas through the construction of roads, infrastructure, and buildings. These developments have disrupted the natural response of dune systems to coastal disturbances, reducing their resilience and increasing the risk of shoreline retreat. Also, the state of the upper limit of the *Posidonia oceanica* meadow may influence sedimentary dynamics acting as a natural

barrier against offshore sediment loss [58]. Where this upper limit is significantly degraded and/or fragmented due to anthropogenic pressures, the system's capacity to preserve morphological equilibrium and resist high-energy events appears to be diminished, thus may result in an increased vulnerability to shoreline retreat (Figure 1). All these factors may interfere with morphodynamic and sedimentary processes and, therefore, affect the position of the shoreline.

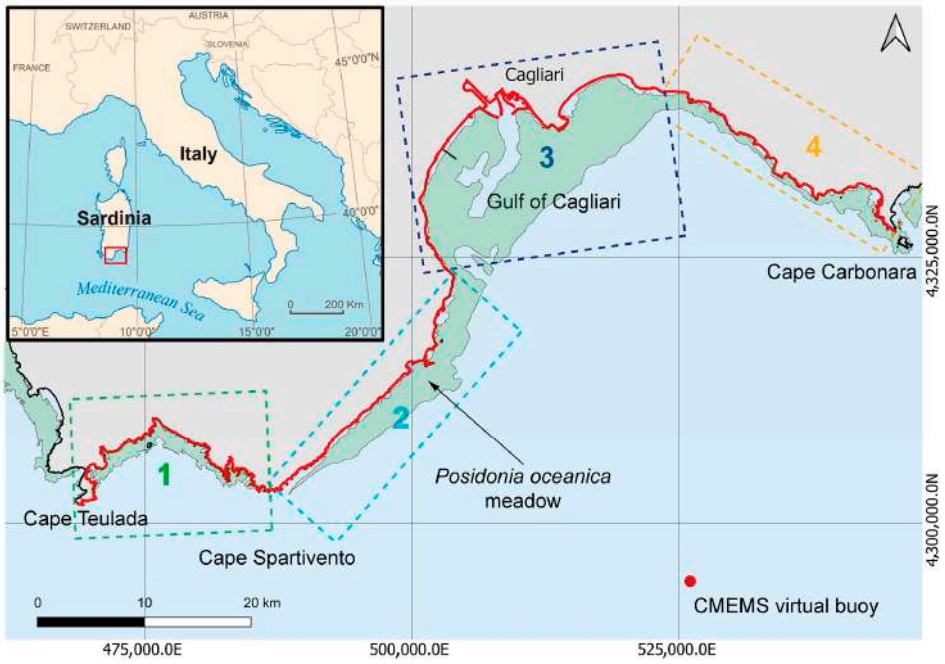

Figure 1. Location of study area: southern coastal stretch of Sardinia Island (Western Mediterranean Sea). The red line highlights the coastal stretch analysed in this study, while the dotted boxes represent the four sectors into which the coastline was subdivided for the data analysis. The *Posidonia oceanica* meadow is marked in green, showing its distribution and proximity to the shoreline in the study area. The red dot indicates the position of the virtual buoy of the Copernicus Marine Environment Monitoring Service (CMEMS). (Coordinate system: UTM 32N; Datum: WGS84).

To facilitate analysis and discussion of the obtained values, the studied coastal stretch area was subdivided into four sectors (Figure 1). Sector 1 extends from Cape Teulada to Cape Spartivento; Sector 2 covers the coastline from Cape Spartivento to the western part of the Gulf of Cagliari; Sector 3 corresponds to the central part of the Gulf of Cagliari; and Sector 4 stretches eastward to Cape Carbonara (Figure 1).

Pocket beaches, or "embayed beaches", are the predominant beach type in Sector 1, which were formed within deep rias inlets resulting from marine ingression into ancient river valleys [59]. Anthropogenic coastal modifications in this sector are minimal, with only a small marina located near a beach east of Cape Teulada.

In Sector 2, the coastline becomes less indented than in Sector 1, with wider beaches interspersed with smaller, more sheltered ones. Moreover, the higher anthropogenic pressure in this sector has led to the construction of coastal engineering structures (e.g., breakwaters, groins, jetties), both parallel and transverse to the shoreline.

In Sector 3, the coastal morphology is more uniform, with long stretched beaches occasionally interrupted and crossed by artificial structures. The urban area of Cagliari, the largest urban centre on Sardinia Island, and its hinterland, where significant urban development has taken place, are included within this sector. This area has undergone substantial modification over the years, primarily due to the construction of marinas, commercial and recreational ports, piers, breakwaters, and other hard coastal defence structures, in addi-

tion to artificial beach nourishments. The presence of transversal groynes and analogous engineering interventions, which are designed to regulate sediment transport and stabilise the coastline, further underscores the significant degree of anthropogenic impact that is characteristic of this central sector [53,60].

Similar to Sector 1, Sector 4 is characterised by small beaches dominated by rocky headlands, occasionally alternating with beaches featuring longer stretches of shoreline. Even in this sector, intense anthropogenic activity has led to the morphological modification of some beaches.

The morphologies observed along the coastline are largely governed by the underlying geology of the study area. Sectors 1 and 4 are both characterised by the presence of Palaeozoic intrusive rocks (mainly granites), linked to the structuring of the Hercynian Basement in Sardinia [61]. However, metamorphic rocks can also be found in Sector 1 [62]. Intrusive rocks are dominant in Sector 2, but a transition to sedimentary deposits (Quaternary) is observed, interrupted by the presence of Oligocene—Miocene volcanic rocks [61]. Finally, the central coastal stretch of the study area (Sector 3) is characterised by the presence of recent post-Hercynian sedimentary cover (Quaternary) [61].

2.2. Shoreline Changes Analysis

The historical shoreline changes (trends of beach accretion and retreat) were performed using the Digital Shoreline Analysis System (DSAS, version 5.1) [47], an add-in of Ersi ArcGIS Desktop software (version 4.10).

For each microtidal beach analysed, shoreline positions were digitalised using aerial orthophotos available in the WMS Service of the Autonomous Region of Sardinia [63], covering a period from 1954 to 2022. Following the works of Usai [52,53], a grid with 4 × 4 km cell size was created to extract the aerial orthophotos, maintaining their original pixel resolution. Overall, 11 aerial orthophoto mosaics were obtained (GeoTIFF format), each corresponding to the year considered for the shoreline analysis (1954, 1968, 1977, 1997, 2003, 2008, 2010, 2013, 2016, 2019, and 2022). To ensure reliable estimates of the shoreline position, all aerial orthophotos were manually georeferenced in a GIS environment to minimise positional errors, using the aerial orthophoto mosaic with the highest resolution and accuracy as a reference (2008). The georeferencing of aerial orthophotos was performed using the polynomial transformation as an interpolation technique.

Shoreline position for each year considered in this study was manually digitalised using QGIS software (version 3.4.10), maintaining a fixed digitisation scale of 1:800. The shoreline position was defined using the instantaneous water line [64,65] as a reference, since this indicator was considered the most suitable given the quality and temporal heterogeneity of some of the earliest photomosaics [65]. Shoreline position measurements are inherently affected by positional uncertainties arising from natural factors that influence shoreline dynamics (e.g., wind, waves, and tides) as well as sampling-related uncertainties, such as digitisation errors and inaccuracies in the image positioning system [65]. Therefore, to improve the accuracy of the results obtained from the shoreline analysis, the values of uncertainties associated with each aerial orthophoto mosaic were estimated. The total positional uncertainty σ_T is described by Equation (1) [66–68]:

$$\sigma_T = \sqrt{\sigma_d^2 + \sigma_p^2 + \sigma_r^2 + \sigma_{co}^2 + \sigma_{wr}^2 + \sigma_{td}^2} \quad (1)$$

where

- σ_d is the Digitisation Error, obtained by digitising the same element (shoreline) 30 times in the same image and calculating the error as the standard deviation of the residual position of that digitised element Table 1,

- σ_p is the Pixel Error, corresponding to the size of one pixel of the image considered Table 1,
- σ_r is the Orthorectification Error, derived from the root mean square error (RMSE) between the image points and their corresponding Ground Control Points (GCPs) Table 1,
- σ_{co} is the Coregistration Error, derived from the root mean square error (RMSE) of residual misalignment among single pixels from the dataset of images considered Table 1,
- σ_{td} is the Tidal Error (derived from the natural fluctuation of sea level), calculated using Equation (2) proposed by Allan [69]:

$$\sigma_{td} = \frac{VC}{S} \quad (2)$$

where VC represents the vertical change in water level and S is the beach slope.

Table 1. Shoreline uncertainties associated with each year of aerial orthophoto considered (from 1954 to 2022), according to Equation (1) (units in metres).

Year	σ_d	σ_p	σ_r	σ_{co}	σ_{wr}	σ_{td}	σ_T
1954	2.86	0.95	3.23	1.64	1.93	1.35	5.27
1968	1.87	0.50	2.13	1.37	1.93	1.35	3.97
1977	1.37	0.52	2.02	1.32	1.93	1.35	3.67
1997	2.19	0.25	1.72	0.99	1.93	1.35	3.79
2003	1.47	1.00	1.03	1.22	1.93	1.35	3.36
2008	0.45	0.10	0.00	0.00	1.93	1.35	2.40
2010	0.89	0.50	1.39	0.51	1.93	1.35	2.96
2013	0.71	0.50	1.07	0.78	1.93	1.35	2.84
2016	0.48	0.20	1.30	0.50	1.93	1.35	2.79
2019	0.57	0.20	0.92	0.59	1.93	1.35	2.67
2022	0.38	0.20	0.79	0.19	1.93	1.35	2.53

Based on data from the tide gauge station located in the Port of Cagliari [70], a tidal range value of 0.35 m was adopted as representative for the study area. To estimate the swash zone slope of each beach, high-resolution LiDAR Digital Terrain Models (DTMs) made available through the Sardegna Geoportale website [71] were analysed. These DTMs were derived from LiDAR surveys conducted by the Italian Ministry for the Environment (MATTM) between 2008 and 2009, on the whole coastal areas of Sardinia. The open-access datasets have a vertical accuracy of 15 cm and a horizontal accuracy of 30 cm. The slope of each beach was calculated, and the corresponding value of σ_{td} was, respectively, determined. The final σ_{td} value used in the analysis was obtained by averaging the individual values derived for each beach (see Table 1).

- σ_{wr} represents the Wave run-up Error, understood as the wet/dry boundary of the swash zone, which was used as a proxy in the multi-temporal shoreline analysis. According to Stockdon [72], the runup elevation ($R_{2\%}$) can be estimated using empirical formula based on the significant wave height in deep water (H_0), the wave period (T), and the beach slope. Based on the analysis of Copernicus Marine Environment Monitoring Service (CMEMS) [73] wave data collected offshore of the study area, a representative value of H_0 = 0.5 m and T = 6.4 s was adopted. Using the previously determined beach slopes, the $R_{2\%}$ value was calculated for each beach, resulting in an average value of $R_{2\%}$ = 0.5 m, which corresponds to a mean shoreline uncertainty of approximately 1.93 m due to wave runup, Table 1.

Finally, the digitalised shorelines and their respective uncertainties were processed using the DSAS tool, estimating the retreat and/or accretion rates of the 79 microtidal beaches under study. More precisely, from a user-defined baseline, a series of equidistant transect perpendicular to the baseline was generated for each beach (with a length of 200 m

and spaced 20 m). For each transect, a suite of statistical indicators was computed in order to analyse the dynamic characteristics of the beaches:

- Shoreline Change Envelope (SCE)—represents the total range of shoreline movement by capturing the maximum distance between all shoreline positions over the considered time period, offering a non-directional measure of total shoreline variability [67,74],
- Net Shoreline Movement (NSM)—measures the total distance of shoreline change between the earliest and the most recent shoreline positions [75],
- End Point Rate (EPR)—calculates the rate of shoreline movement by measuring the change between the earliest and most recent shoreline positions over the considered time period [76,77],
- Weighted Linear Regression (WLR)—assigns variable weights to shoreline positions based on their temporal spacing and positional uncertainty, giving greater influence to measurements with higher accuracy. In DSAS, weights are typically calculated as the inverse of the squared positional error, thus helping to reduce the impact of less reliable data. This approach improves the robustness of trend estimation in heterogeneous datasets and is particularly effective when shoreline records vary in quality or temporal distribution [65,78],
- Linear Regression Rate (LRR)—is calculated by fitting a least-squares linear regression line through all shoreline positions, providing a robust estimate of long-term trends in shoreline movement [79,80]. However, the values obtained for the LRR were not reported in the results figures in order to avoid repeating two linear regression values, giving priority to those weighted with uncertainty values (WLR).

Moreover, the maximum cross-shore width of each beach has been digitised using the 2022 aerial orthophotos. This has been performed in order to facilitate correlation with the statistical indices listed above.

2.3. Wave Storm Events Analysis

To assess the potential impact of wave storm events on beach morphodynamics over the years, CMEMS reanalysis data were analysed for the study area [73]. For this purpose, the computational grid located offshore of the study area was selected, and wave parameters were extracted from 1 January 1985 to 31 December 2022 from the virtual buoy indicated by the red dot in Figure 1. In particular, the significant wave height (H_s) and wave direction (θ) were extracted. Wave storm events were identified using the Peak Over Threshold (POT) approach [81], which selects all sea states where the significant wave height (H_s) exceeds a fixed threshold of 1 m for a minimum continuous duration of 6 h. To avoid double-counting recurrent peaks within the same storm, consecutive peaks were merged if they occurred within a time gap of 48 h. For each identified event, the following parameters were computed:

- Maximum significant wave height (H_{smax}; metres)
- Duration of the storm events (D; hours)
- Mean wave direction, computed using the circular mean equation (Equation (3)) to account for the directional nature of the data ($\bar{\theta}$ degree):

$$\bar{\theta} = \text{atan2}\left(\sum_{i=1}^{n} sin(\theta_i),\ \sum_{i=1}^{n} cos(\theta_i)\right) \quad (3)$$

where θ is the wave direction of each record in radians. The resulting mean direction was then converted back to degrees and normalised in the interval [0°, 360°].

For each storm event identified through POT analysis, the storm power index P_s (m^2h) was also calculated [82,83]. This index is a function of both the maximum significant wave height and the duration of the storm and is considered an appropriate parameter for defining the strength of a storm. In this study, the storm power index (Equation (4)) was used as a proxy for the potential erosive power of each storm event.

$$P_s = H_{smax}^2 D \quad (4)$$

where H_{smax} is the maximum significant wave height for each storm (m), and D is the storm event duration (h).

3. Results and Discussion

The study area is located along the southern beaches of Sardinia, covering a coastline of approximately 180 km in length. Of this, approximately 52 km consists of the 79 beaches analysed over a period of approximately 70 years. Depending on the DSAS processing, a total of 2573 transects were used for the SCE, NSM and EPR calculations, while the number decreased to 2568 transects for the LRR and WLR analyses due to the incomplete overlap of all historical datasets on the coastline. The values of the statistical indicators obtained are reported in Tables A1–A4 (See Appendix A).

The Shoreline Change Envelope (SCE) analysis revealed an average variability of 24.1 m along the study area, with maximum values reaching 135.4 m in Sector 3 (Figure 2, Beach ID 47 in Table A3), while minimum values of 0.7 m were recorded in Sector 4 (Figure 2; Beach ID 58 in Table A4).

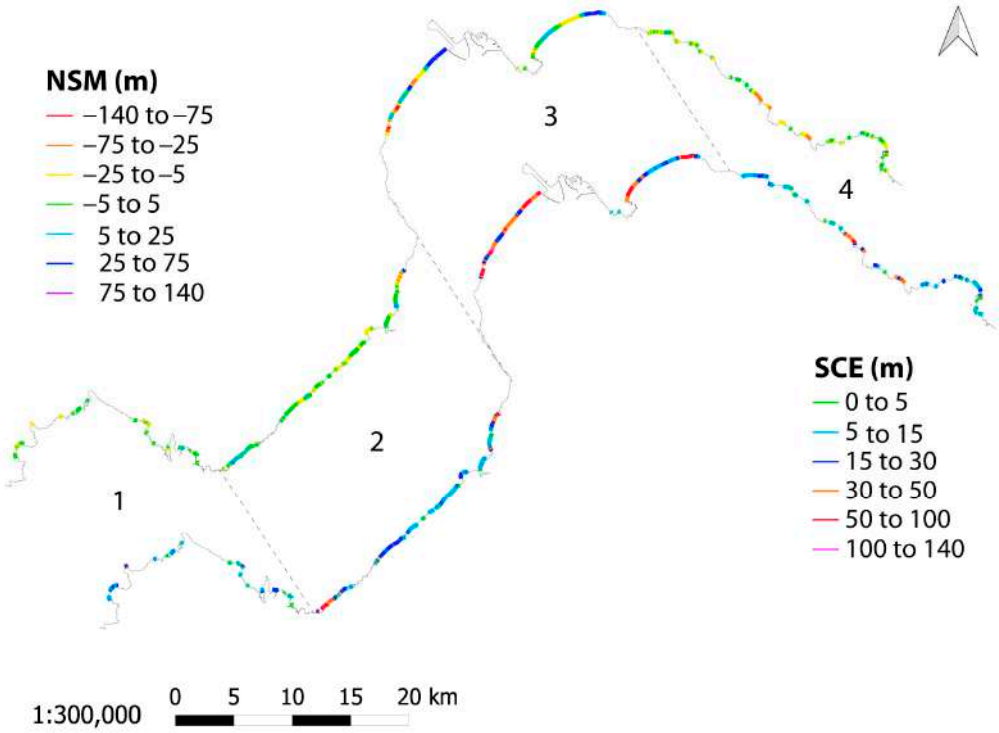

Figure 2. Graphical representation of the entire study area of the calculated NSM and SCE indicators. For ease of presentation, the four sectors of the study area are also shown.

The Net Shoreline Movement (NSM) analysis indicates an average shoreline retreat of −1.47 m along the study area. Overall, 1631 transects (63.4% of the total) show negative distance values, indicating net retreat, while 942 (36.6% of the total) display positive values, reflecting local accretion. The maximum shoreline retreat was recorded in Sector 3 with a

value of −132.2 m (Figure 2; Beach ID 47 in Table A3), whereas the maximum shoreline accretion was observed in Sector 4 with a positive distance of 108.1 m (Figure 2; Beach ID 75 in Table A4).

The End Point Rate (EPR) analysis indicates an overall condition of substantial stability along the study area, with an average rate of −0.02 m/yr. However, 1631 transects (63.4% of the total) have a retreating trend, while 34.7% of the total transects exhibit statistically significant retreat rates, with maximum values reaching −1.9 m/yr in Sector 3 (Beach ID 47 in Table A3). Conversely, 942 transects (36.6% of the total) have an accretional rate, while 20.5% of the total transects exhibit statistically significant accretion, and maximum positive rates of 1.59 m/yr are recorded in Sector 4 (Beach ID 75 in Table A4).

Average values of Weighted Linear Regression (WLR) indicate an overall stability for the entire study area, with a mean rate of −0.02 m/yr. However, 67 beaches (84.8%) exhibit a negative rate (retreat), while 12 beaches (15.2%) display a positive trend (accretion). Of all transects, 1708 (66.5% of the total) show a retreating trend, while 23.8% are in statistically significant retreat, with a maximum rate of −1.59 m/yr recorded in Sector 3 (Beach ID 47 in Table A3). Conversely, 860 transects (33.5% of the total) are in an accretional trend, while a total of 12% of the transects exhibit statistically significant accretion, with a maximum rate of 1.94 m/yr calculated in Sector 4 (Beach ID 75 in Table A4). When considering natural beaches from those influenced by the presence of anthropogenic structures, for natural beaches the average retreat rate is −0.07 m/yr and the average accretion rate is 0.05 m/yr. In contrast, anthropised beaches show an average retreat rate of −0.33 m/yr, while an average accretion rate of 0.22 m/yr.

Average values of Linear Regression Rate (LRR) obtained for the entire study area indicate an average rate of −0.01 m/yr. 1615 transects (62.9% of the total) are in retreating trend, while 29.1% show statistically significant retreat, with a maximum rate of −1.76 m/yr recorded in Sector 3 (Beach ID 47 in Table A3). On the other hand, 953 transects (37.1% of the total) are in accretional rate, while 14.2% show statistically significant accretion, with a maximum rate of 1.58 m/yr calculated in Sector 4 (Beach ID 75 in Table A4).

Across the study area, the comparison between maximum beach width (digitalised from 2022 aerial orthophotos) and the Shoreline Change Envelope (SCE) highlights clear differences between anthropised beaches (red dots in Figure 3) and natural beaches (green dots in Figure 3). Anthropised beaches, influenced by structures such as groynes, harbours, and marinas, show widths mostly between 10 and 50 m (only one reaching about 120 m), whereas natural beaches range approximately from 10 to 70 m (only two exceeding 100 m).

Natural beaches display lower SCE values, reflecting their greater capacity for resilience and self-regulation. Here, a moderate correlation between maximum beach width and SCE was found (R^2 = 0.49). In contrast, anthropised beaches show higher SCE variability, no maximum beach width—SCE correlation (R^2 = 0.001), and more persistent shoreline changes, as structures constrain natural recovery. In cases where SCE exceeded 60 m, harbour and groyne construction produced substantial accretion or retreat, often preventing the shoreline from returning to its original position.

Overall, these variations can be primarily attributed to local specific factors and these findings highlight the importance of integrating anthropogenic influences when analysing shoreline evolution, as localised deviations from general trends may reflect complex interactions that cannot be fully explained through a large-scale approach. To better illustrate these observations, each sector has been further described below.

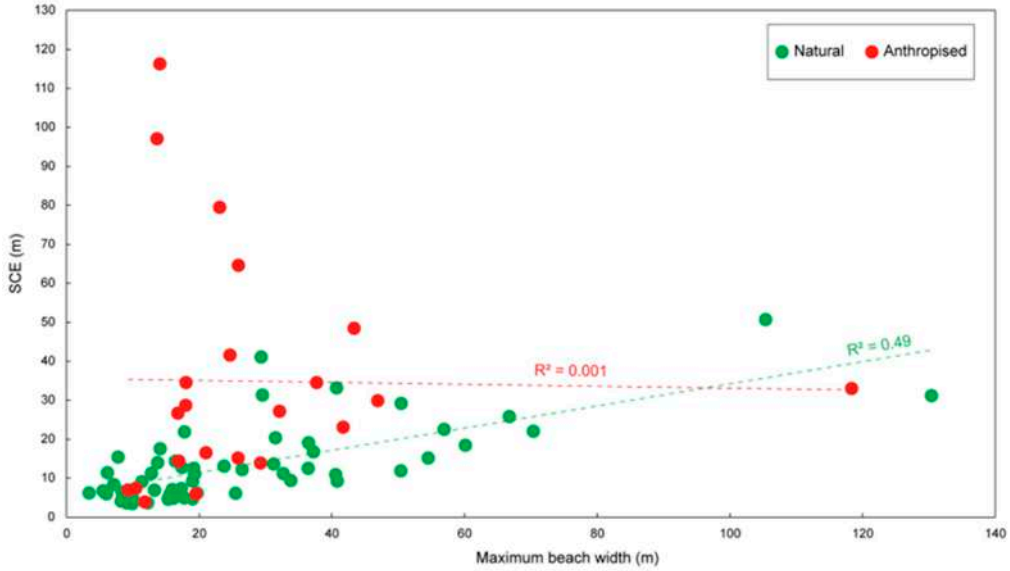

Figure 3. Correlation between the statistical indicator SCE (Shoreline Change Envelope) and the maximum beach width, considering natural beaches (green dots) and anthropised beaches (red dots).

3.1. Sector 1

The coastal stretch of sector 1 is characterised by the least anthropogenic changes in the entire study area, which is also reflected in the overall stability of the coastline. In this sector, the highest SCE values were recorded at Beaches ID 3, 11 and 17. The values and trends (shoreline retreat and accretion) associated with SCE, NSM, EPR and WLR statistical indicators are reported in Figures 4 and 5.

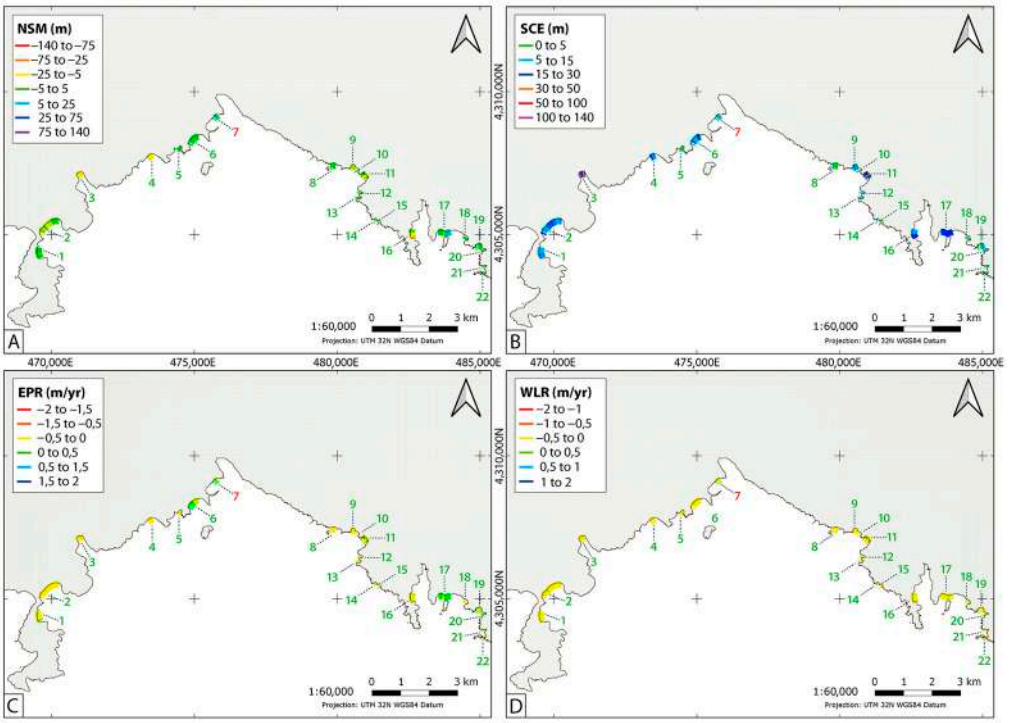

Figure 4. Values of the statistical indicators (**A**) NSM, (**B**) SCE, (**C**) EPR, and (**D**) WLR for each transect of beaches identified in Sector 1. The colour of the beach identification number indicates its type: natural (green number) or anthropised (red number). Coordinate system: UTM 32N; Datum: WGS84.

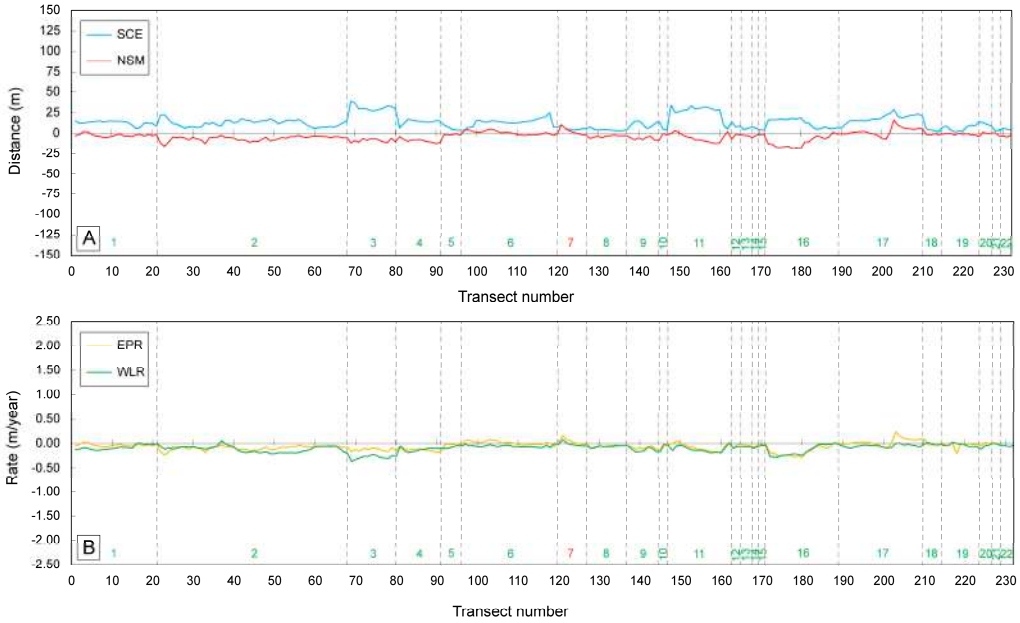

Figure 5. Values of the statistical indicators measured for each beach in Sector 1: (**A**) SCE and NSM; (**B**) EPR and WLR. The colour of the beach identification number indicates its type: natural (green number) or anthropised (red number).

For Beach ID 3 (Porto Scudo beach), a relatively high SCE value was recorded, together with a retreating WLR rate of −0.36 m/yr, the lowest calculated in this sector. This localised retreat trend is likely related to the repeated military exercises regularly conducted on Beach ID 3, which is located within the military training area of Cape Teulada, active since 1956. This beach is periodically used for manoeuvres with heavy vehicles and amphibious landing operations (Figure 6A,B). Orthophoto analysis clearly illustrates the visible impacts of these activities on the entire beach system, including the flattening of natural beach morphologies and the fragmentation of the foredune ridge, both of which compromise the system's natural resilience to storm events. The removal of micro topographic features and damage to the dune structure reduce the beach's capacity to trap and retain sediment, making it more vulnerable to episodic retreat. This combination of factors can explain the recorded retreat rate and highlights the importance of considering human impacts on coastal stability, especially in otherwise natural sectors.

On the other hand, the high SCE values (maximum value of 34.1 m) recorded for Beach ID 11 (Piscinnì beach) are mainly related to the natural dynamics of sedimentation and erosion of large volumes of *Posidonia oceanica* rests (commonly known as banquettes [34,54]). In fact, due to a coastal video monitoring system installed in 2011, it has been observed that after the most intense storm events, which reach the foredune, the deposition of banquettes plays a key role in restoring the shoreline position, leading in some cases to accretion of up to 30 m following major storms [55]. Moreover, these accumulations tend to intensify along the beach extremities, promoting periodic shoreline rotation and shifting sediment along the cuspate margins of the system [55]. This natural cycle of banquette deposition acts as a buffer against storm impacts by reinforcing parts of the foreshore, but when the accumulation is uneven, it can shift wave energy towards unprotected sections, resulting in localised retreat. This mechanism helps explain why positive NSM values occur at the beach extremities, while the central area shows slightly negative trends.

Finally, for Beach ID 17 (Tuerredda beach) (Figures 4 and 5), the marked coastline variability, together with the coexistence of sections undergoing retreat and accretion, can be attributed to its cuspid morphology, which makes this beach particularly susceptible to coastline rotation over time, with an average value of WLR of −0.04 m/yr.

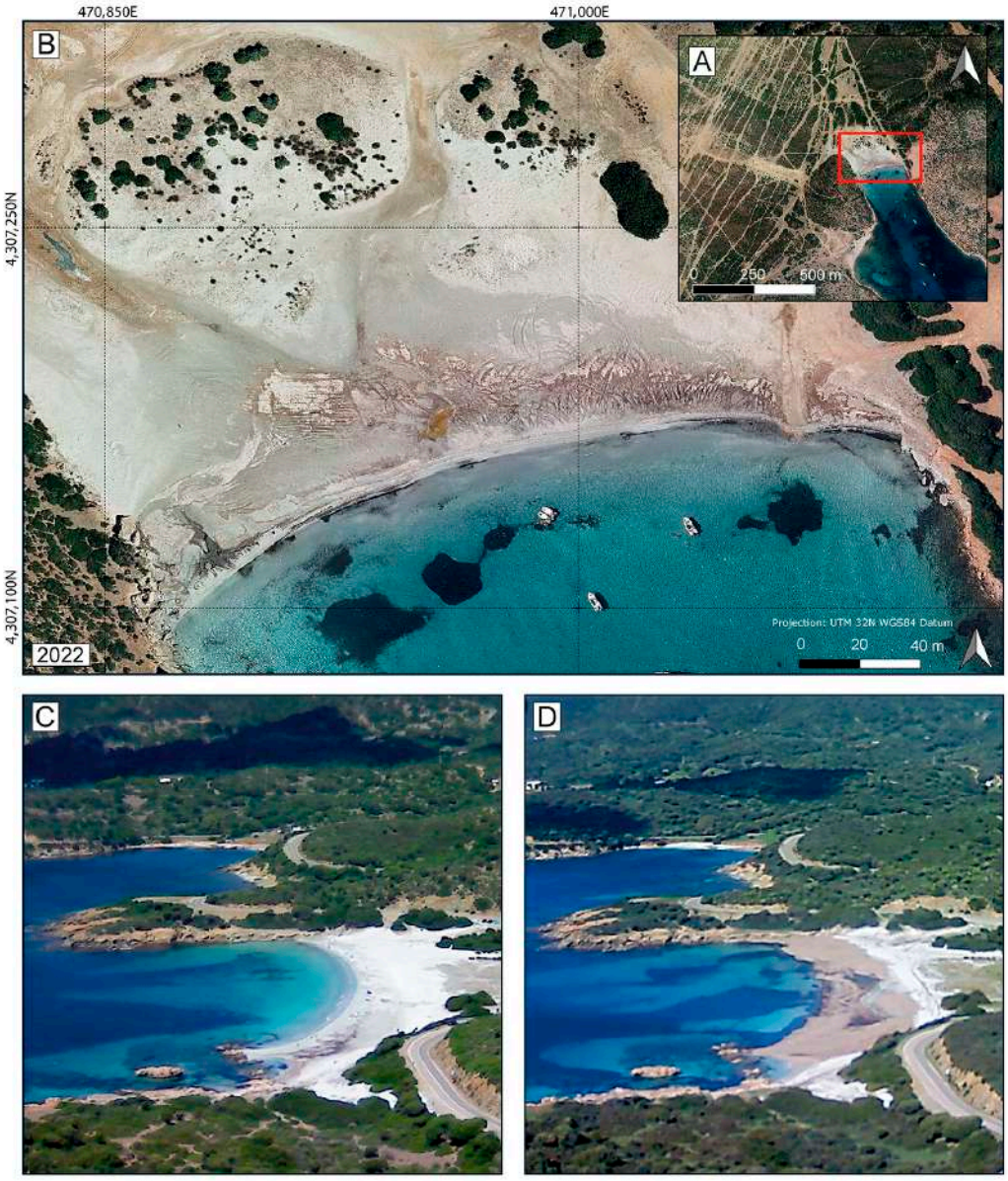

Figure 6. Panel (**A**,**B**) show Beach ID 3 (Porto Scudo beach). This beach falls within the military area of Capo Teulada, and the marks left on the entire dune system by the continuous transit of heavy military vehicles are evident (Panel (**A**)), while during more intense exercises, with amphibious vehicles landing on the beach, all the natural features of the exposed beach are completely flattened, further widening the gaps in the foredunes and compacting the sand, predisposing the beach to retreat processes (Panel (**B**)). Coordinate system: UTM 32N; Datum: WGS84. Panels (**C**,**D**) come from the coastal video monitoring system installed at Beach ID 11 (Piscinnì beach). The deposition of large quantities of *Posidonia oceanica* banquettes makes the position of the shoreline highly variable on this beach.

3.2. Sector 2

Similarly to Sector 1, Sector 2 shows an overall condition of relative shoreline stability. The values and trends (shoreline retreat and accretion) associated with SCE, NSM, EPR and WLR statistical indicators are reported in Figures 7 and 8. Maximum SCE values were recorded at Beaches ID 24 and 41 (Figures 7 and 8).

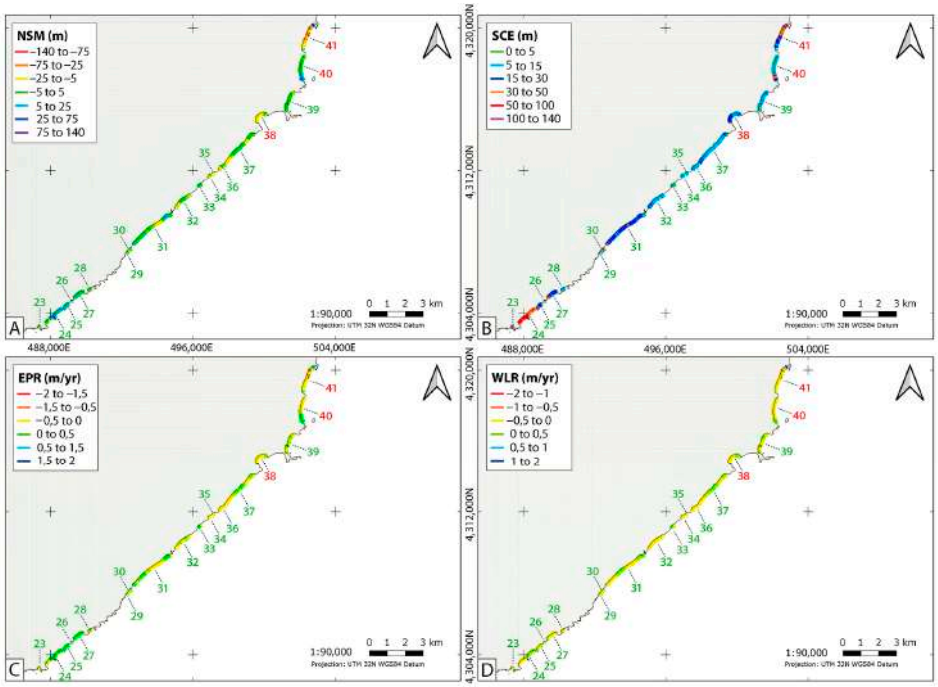

Figure 7. Values of the statistical indicators (**A**) NSM, (**B**) SCE, (**C**) EPR, and (**D**) WLR for each transect of beaches identified in Sector 2. The colour of the beach identification number indicates its type: natural (green number) or anthropised (red number). Coordinate system: UTM 32N; Datum: WGS84.

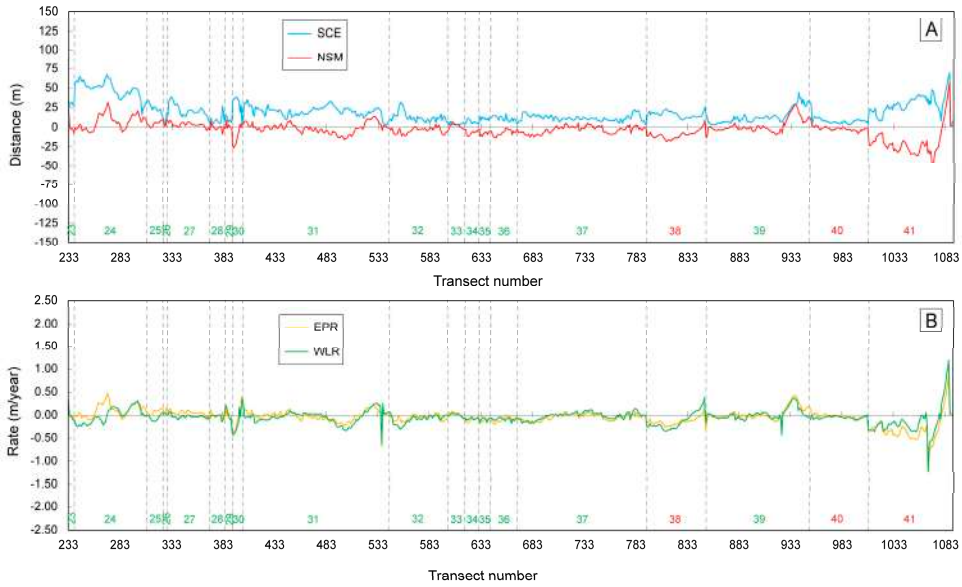

Figure 8. Values of the statistical indicators (**A**) SCE and NSM, (**B**) EPR and WLR for each transect of beaches identified in Sector 2. The colour of the beach identification number indicates its type: natural (green number) or anthropised (red number).

Beach ID 24 (Su Giudeu beach) shows a maximum SCE value of 68.0 m, a maximum NSM value of 32.0 m and a maximum WLR trend of 0.31 m/yr, which are the highest values recorded among the natural beaches in this sector. This notable shoreline mobility can be attributed to the interaction of three main factors: (1) the large amount of sediment stored in the extensive backshore dune system, which provides a substantial sediment reservoir for natural redistribution; (2) its cuspate morphology, which makes the shoreline particularly sensitive to changes in wave direction and intensity; (3) the presence of a pond that periodically discharges into the sea depending on rainfall, introducing additional

variability to sediment supply and local hydrodynamics (Figure 9A,B). As a result, intense storm events are capable of eroding the foredune, causing short-term shoreline retreat, as demonstrated by the comparison between the 2008 and 2022 orthophotos (Figure 9A,B). Nevertheless, when longer time frames are considered, such as the period from 1954 to 2022, the shoreline shows an overall trend towards accretion. This indicates that, despite episodic retreat events, the natural sediment dynamics and dune supply maintain the beach system's capacity to recover over the long term, underlining the importance of preserving dune connectivity and natural buffers in coastal management strategies.

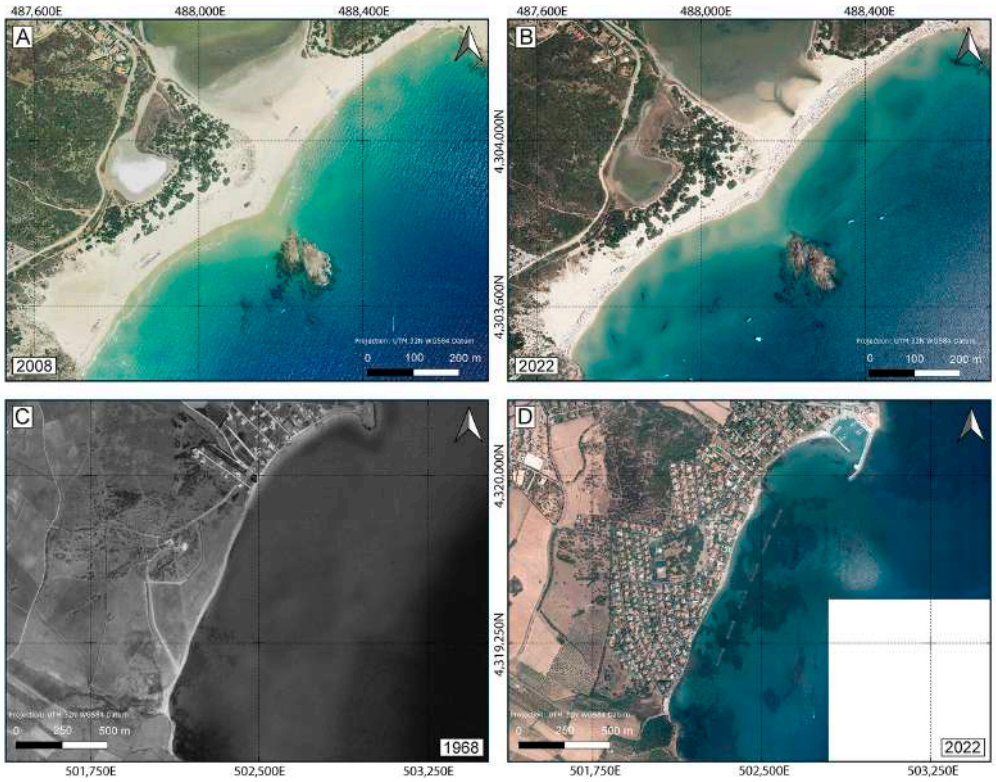

Figure 9. Panels (**A**,**B**) show Beach ID 24 (Su Giudeu beach). The cusp-shaped nature of this beach, together with the large amount of sediment accumulated in the dune system and the presence of the pond, may explain the high variability of the shoreline at this beach, which shows areas of accretion and areas of retreat. Panels (**C**,**D**) show Beach ID 41 (Perd'e Sali beach). The construction of a marina and the installation of groynes parallel to the shoreline have altered the local currents at this beach, creating areas of severe retreat and others with moderate accretion. Coordinate system: UTM 32N; Datum: WGS84.

In contrast, Beach ID 41 (Perd'e Sali beach) shows clear signs of alteration due to anthropogenic interventions: 85.5% of its transects show negative NSM values, with 48.2% of transects showing statistically significant retreat according to the WLR indicator, reaching maximum negative NSM values of −46.2 m and maximum negative WLR trend of −1.22 m/yr (Figures 7 and 8). However, the easternmost portion of this beach shows positive shoreline change, with a maximum NSM value of 57.4 m, a maximum WLR trend of 1.2 m/yr (9.6% of transects indicating statistically significant accretion). This localised shoreline retreat and accretion are likely attributable to the construction of a marina and coastal defence structures (groynes parallel to the shoreline) built in this area between 1977 and 1997. These engineering interventions may have disrupted natural longshore sediment transport, potentially leading to sediment trapping and obstruction. Such alterations could intensify shoreline retreat in downdrift areas deprived of sediment supply, while favouring localised accretion immediately updrift of the structures. The high

degree of human modification and urbanisation might further limit the beach's capacity to recover from extreme events, restricting sediment redistribution and dune development (Figure 9C,D). Consequently, the beach may exhibit a persistent erosional trend, suggesting the need for integrated management strategies that safeguard sediment connectivity and system resilience.

3.3. Sector 3

Figures 10 and 11 show the values and spatial–temporal trends of shoreline retreat and accretion, as derived from the SCE, NSM, EPR and WLR statistical indicators, for sector 3. This is the area of the studied coastline that has been most affected by anthropogenic modifications. This sector includes the metropolitan area of Cagliari city (Figure 1), including several urban beaches, extensive hard coastal defence structures and a large port area.

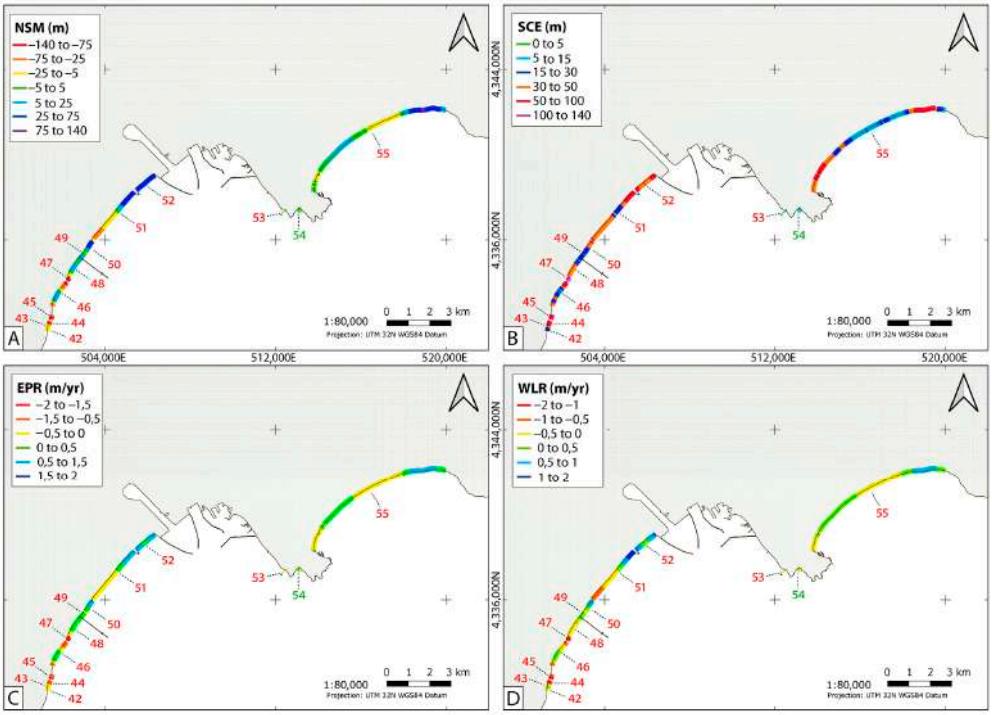

Figure 10. Values of the statistical indicators (**A**) NSM, (**B**) SCE, (**C**) EPR, and (**D**) WLR for each transect of beaches identified in Sector 3. The colour of the beach identification number indicates its type: natural (green number) or anthropised (red number). Coordinate system: UTM 32N; Datum: WGS84.

The highest values of SCE in the entire study area are recorded in this sector, reaching 135.4 m (La Maddalena beach, ID 47), which corresponds in this beach to a minimum NSM value of −132.2 m and a minimum WLR rate of −1.6 m/yr (Figures 10 and 11). A similar trend was observed for Beaches ID 43 and 44, both bounded by groynes oblique to the shoreline. These engineering structures were originally designed to protect coastal buildings and infrastructure from direct erosion. However, these structures have had a significant impact on the local sediment dynamics. The groynes may have altered the natural longshore current, which in this area flows mostly from south to north [84]. This could lead to the formation of small circulation cells that trap and redirect sediment transport processes. Furthermore, the groynes contributed to the erosion of the original beach within these constructions, with progressive sediment loss and shoreline retreat. Indeed, these beaches recorded maximum SCE values of 94.8 m and 105.1 m, respectively, and minimum NSM values of −94.1 m and −96.1 m (indicating substantial net shoreline

retreat). The WLR trends for these beaches confirm this pattern, with average value rates of −0.78 m/yr (Beach ID 43) and −1.32 m/yr (Beach ID 44) (Figure 12A,B).

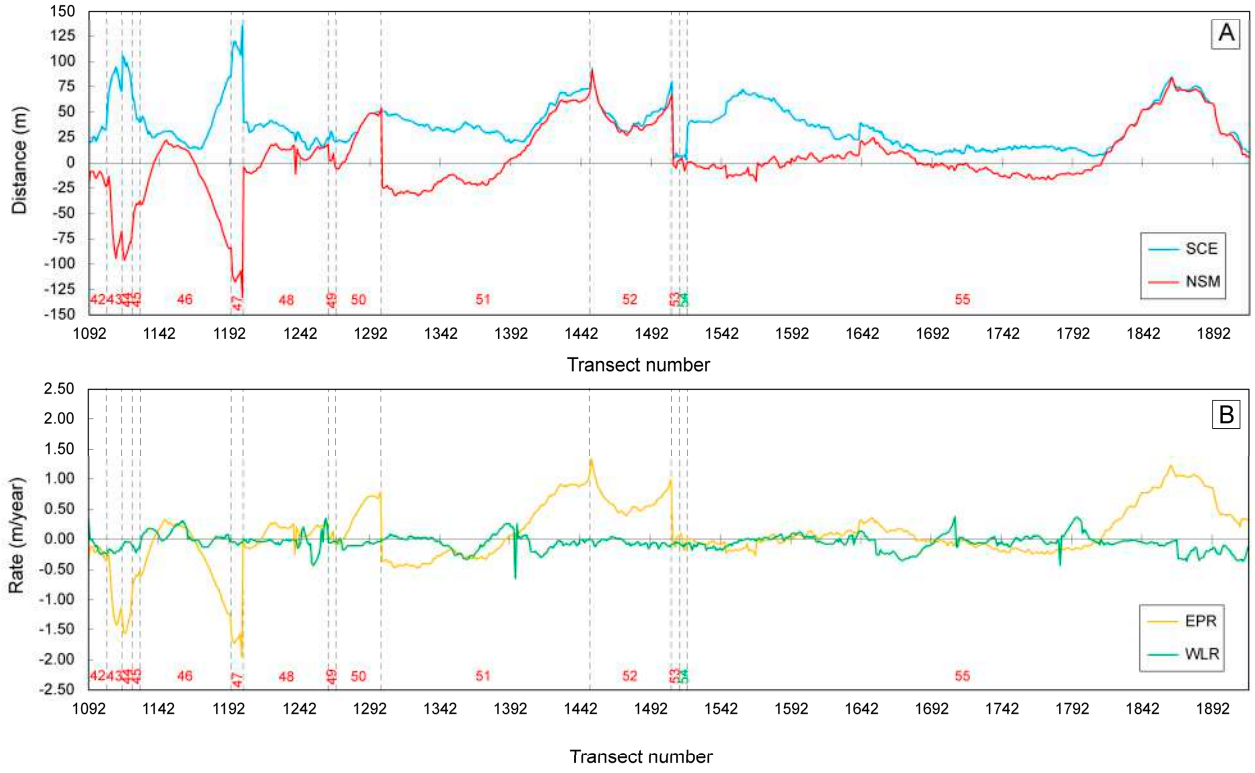

Figure 11. Values of the statistical indicators measured for each beach in Sector 3: (**A**) SCE and NSM; (**B**) EPR and WLR. The colour of the beach identification number indicates its type: natural (green number) or artificial (red number).

Figure 12C shows another example of recent shoreline modification caused by rigid coastal structures. This can be seen at the boundary between Beaches ID 50 and ID 51 (both commonly referred to as Giorgino Beach), which is defined by two jetties built perpendicular to the shoreline. These jetties allow for the passage of a channel that connects to the lagoon behind. The presence of these structures here also interrupts the natural longshore sediment transport, creating an updrift area characterised by pronounced sediment accumulation and accretion. This corresponds to a maximum SCE value of 54 m, which is fully reflected in positive maximum NSM values of 54 m in Beach ID 50. In contrast, the downdrift side exhibits a clear sediment deficit; the beach is unable to naturally recover after major storm events, resulting in progressive retreat. This process may be further exacerbated by the degradation of the *Posidonia oceanica* meadow in front of these beaches (from Beach ID 42 to Beach ID 52), which is no longer able to effectively mitigate wave energy and prevent sediment loss offshore. The consequence of this process is that Beach ID 51 records maximum negative NSM values of −32.8 m, with maximum SCE values of 75.7 m. This shoreline retreat made it necessary to build a seawall to protect the road that runs between the beach and the lagoon behind it (Figure 12C). [28,60]

Finally, Beach ID 55 (Poetto beach) has undergone various anthropogenic modifications over time [28]; among them was a beach nourishment carried out in the early 2000s along the south-western area of the beach, particularly around transect no. 1555 (Figure 13). This intervention resulted in a maximum SCE value of 72.4 m and a minimum NSM value of −15.4 m in the nourished area (Figures 10 and 11).

Despite the absence of evident coastline retreat, as evidenced by analysis of coastline positions mapped between 1954 and 1998 (see Figure 13D), large-scale beach nourishment

was undertaken in 2002. This involved the deposition of approximately 300,000 m^3 of sand, which differed significantly in grain size and composition from the native sediments [85,86]. This intervention resulted in substantial alterations to the local morphology and morphodynamics of the beach [86]. The consequence of this phenomenon resulted in a sudden accretion of more than 60 metres of the shoreline, as evidenced by the 2003 orthophotos. However, this state of disequilibrium led to the rapid retreat of the added material. By 2010, the coastline had undergone a retreat of approximately 50 metres from its 2003 position at transect 1555 (see Figure 13C,D). Twenty years after beach nourishment, analysis shows that the coastline in this area has essentially returned to its pre-beach nourishment position in 1997.

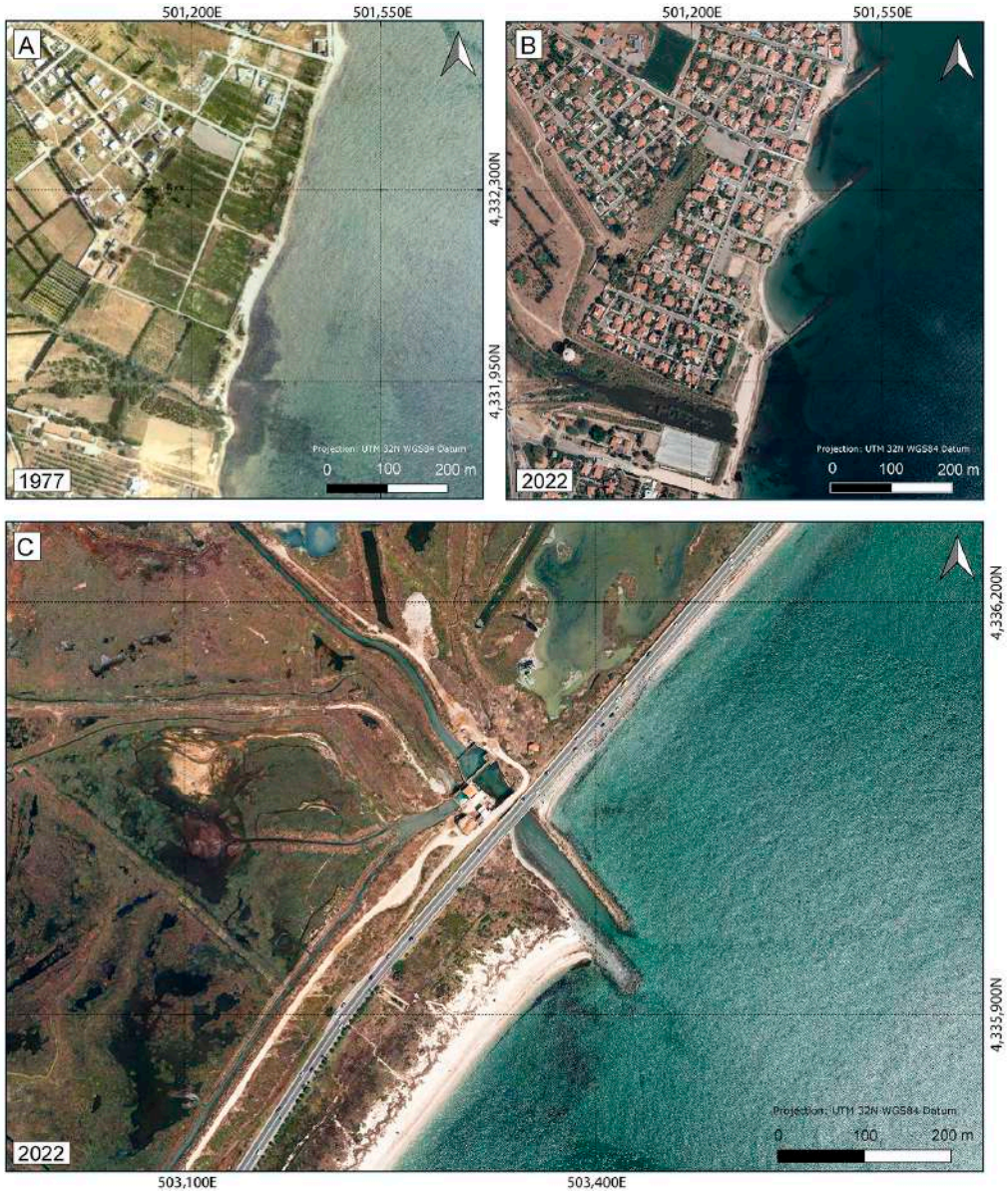

Figure 12. Panels (**A**,**B**) show beaches ID 43 and 44 (Frutti d'Oro Beach), which are bordered by oblique groynes that have caused severe retreat. Panel (**C**) shows how the construction of two jetties across beaches ID 50 and 51 has interrupted longshore sediment transport, creating significant accretion in the updrift zone and significant retreat in the downdrift zone. Coordinate system: UTM 32N; Datum: WGS84.

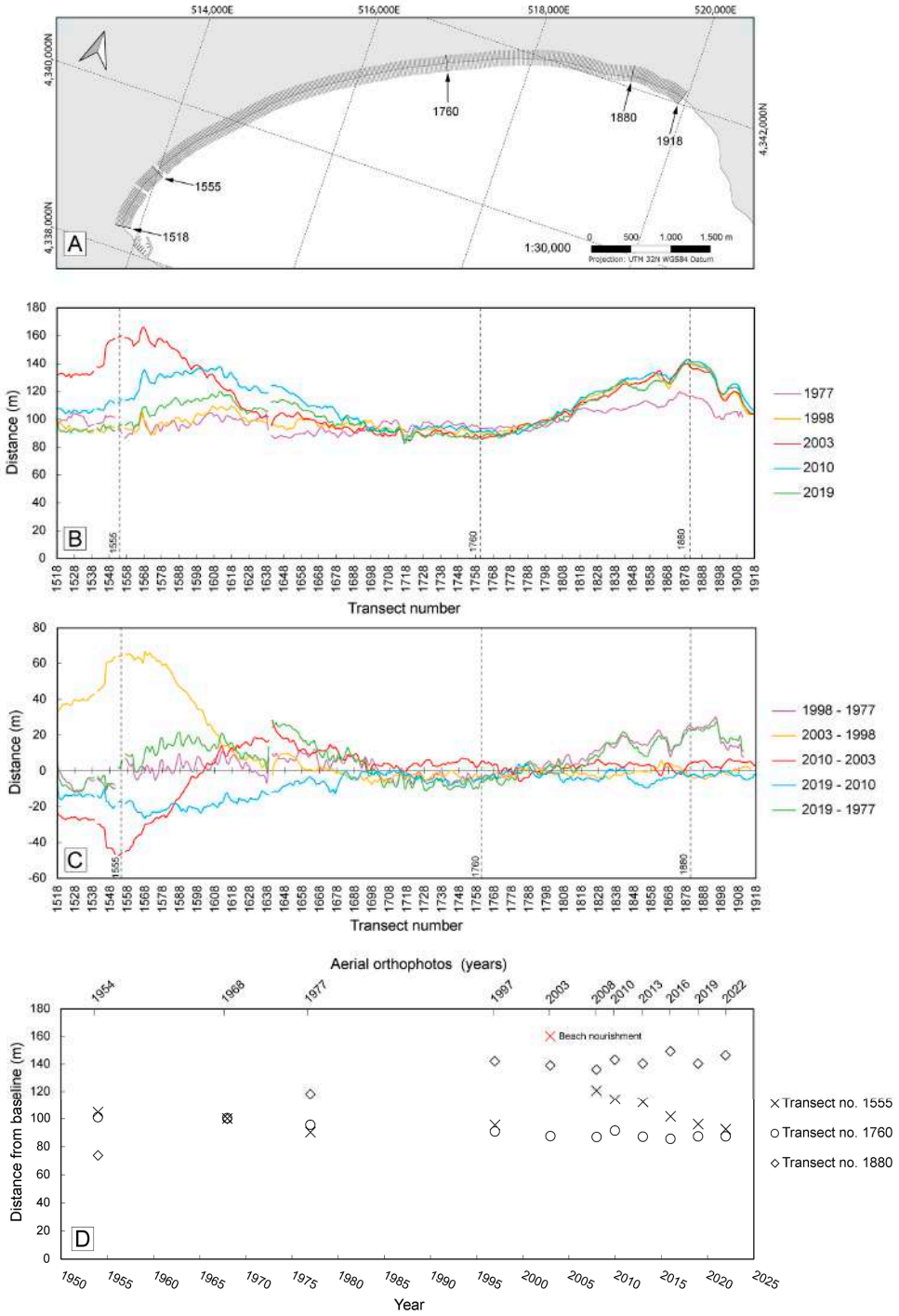

Figure 13. Evolutionary trends of Beach ID 55 (Poetto beach). Panel (**A**) shows the location of the transects used to calculate the DSAS statistical indicator. Coordinate system: UTM 32N; Datum: WGS84. Panel (**B**) shows the shoreline distance from the baseline over time, while Panel (**C**) highlights the changes in shoreline positions across different time intervals. Panel (**D**) shows in detail the temporal variation in shoreline distance from the baseline for transects 1555 (cross symbols), 1760 (circle symbols), and 1880 (square symbols). Transect 1555 experienced a marked accretion immediately after the nourishment, followed by rapid retreat that returned the shoreline to its 1997 position. On the other hand, transect 1760 does not appear to have benefited from the sediment input provided by the nourishment, maintaining a relatively stable shoreline position over time. Finally, transect 1880 shows an unexpected increase of approximately 70 m in shoreline position between 1954 and 1997, which has subsequently remained essentially unchanged to the present day.

Analysis of transect 1760, located in the middle of Beach ID 55, further confirms this: here, the shoreline has remained stable, with no significant accretion from the longshore transport of nourished material (Figure 13D).

Moreover, at transect 1880 in the north-eastern sector of Beach ID 55, a steady accretion trend was recorded from 1954 to 1997 (Figure 13D), after which it stabilised. However, further site-specific studies and analyses would be required to gain a detailed understanding of the processes driving this trend.

3.4. Sector 4

In Sector 4, the extent of anthropogenic modifications to the shoreline is generally lower than in Sector 3. Figures 14 and 15 show the values of the statistical indicators SCE, NSM, EPR and WLR for this sector.

Where anthropogenic modifications are present, such as at Beach ID 57 (Capitana Beach) and Beach ID 75 (Spiaggia del Riso Beach), maximum SCE values of 44.6 m and 119.9 m are recorded, respectively (Figures 14 and 15). In both cases, the construction and/or expansion of small marinas has significantly altered local coastal currents and disrupted natural sediment transport processes. These interventions have led to substantial changes in the adjacent beaches, with some stretches experiencing pronounced shoreline retreat, while others display clear signs of localised accretion (Figure 15). Such contrasting patterns demonstrate how even relatively small-scale coastal infrastructure can exert considerable influence on sediment dynamics when implemented in morphologically sensitive areas.

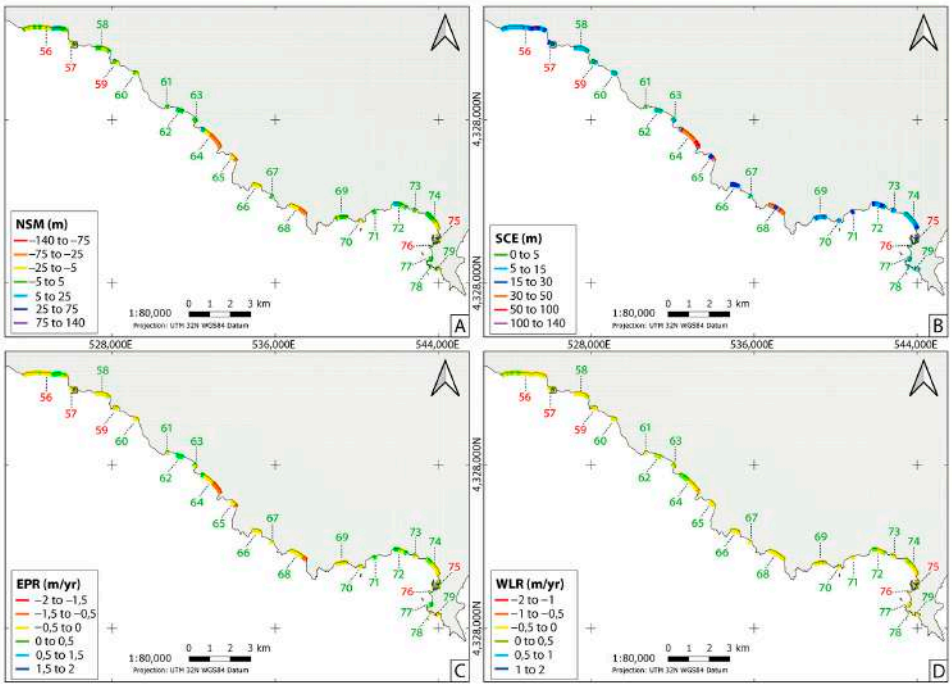

Figure 14. Values of the statistical indicators (**A**) NSM, (**B**) SCE, (**C**) EPR, and (**D**) WLR for each transect of beaches identified in Sector 4. The colour of the beach identification number indicates its type: natural (green number) or anthropised (red number). Coordinate system: UTM 32N; Datum: WGS84.

A different set of processes appears to influence the patterns recorded at Beaches ID 64 (Kal'e Moru), 65 (Cann'e Sisa), 68 (Solanas), and 74 (Campulongu). These beaches share a similar shoreline orientation, ranging between 120° N and 135° N, which exposes them to the same dominant wave directions, see Figure 14. This common exposure results in marked

morphological variability and distinct spatial patterns of shoreline change. Specifically, these beaches exhibit significant retreat in their south-eastern sectors, with maximum negative shoreline change values (NSM) of −55.9 m (Beach ID 64), −46.6 m (Beach ID 65), −47.0 m (Beach ID 68), and −15.0 m (Beach ID 74). Conversely, their north-western areas tend to be more stable or show lower retreat rates, sometimes even slight accretion, with NSM values of 19.9 m in Beach ID 64, −20.2 m in Beach ID 65, −13.4 m in Beach ID 68, and 2.6 m in Beach ID 74 (Figures 14 and 15). These patterns reflect the influence of similar wave dynamics combined with local geological controls, such as headland orientation, on coastal processes across the beaches. In order to better understand this spatial variability, a Peaks Over Threshold (POT) analysis of significant storm events was carried out using data from a virtual CMEMS reanalysis buoy covering the period 1985–2022

From the POT analysis, a total of 1161 storm events exceeding the defined thresholds were identified, averaging approximately 31 events per year. The data analysis shows that the most intense year was 1987, which recorded 27 events with a mean value of storm power index (P_s) equal to 2520 m^2h and an average direction of 221°. In contrast, the least intense year was 1994, with 36 events in total and a mean P_s value of 514 m^2h and an average direction of 248°.

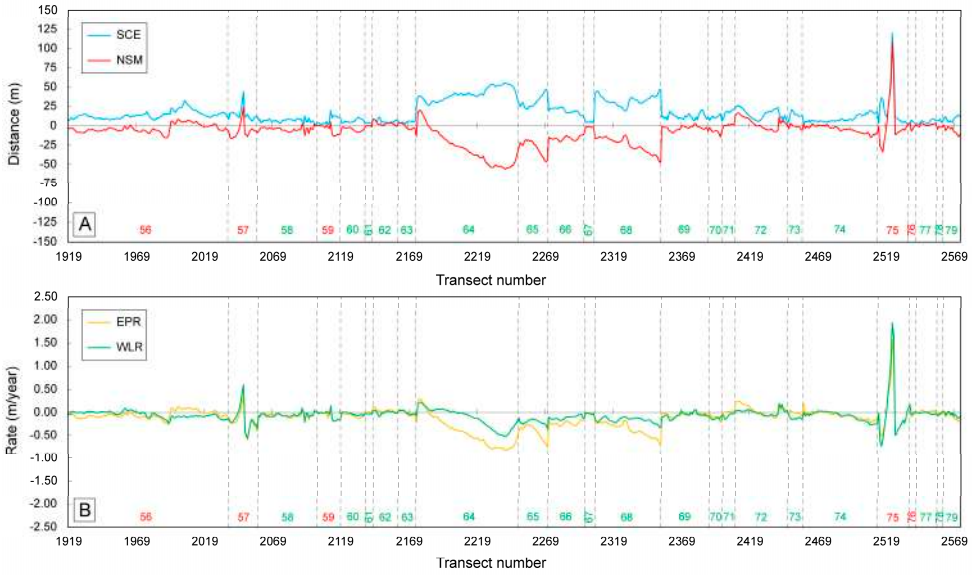

Figure 15. Values of the statistical indicators measured for each beach in Sector 4: (**A**) SCE and NSM; (**B**) EPR and WLR. The colour of the beach identification number indicates its type: natural (green number) or anthropised (red number).

The analysis of mean wave directions reveals a marked predominance of events from sectors between 250° N and 290° N (Figure 16), which are associated with the highest values of storm power index within the analysed time series. In fact, 447 events originate from these directions, equal to 38.5% of the total, with a mean value of P_s equal to 1279.8 m^2h. The maximum computed value of P_s has been reached in January 1987 (46248 m^2h) with a mean wave direction of 273° N, maximum H_s of 7.3 m and a duration of 861 h. Similarly oriented headlands modulate sediment transport patterns, promoting shoreline retreat on the wave-exposed sides and accretion on the sheltered sides. The interaction between incident wave energy, embayment geometry and local morphological setting has been shown to promote the development of longshore currents, leading to intensified shoreline retreat in high-energy sectors. Conversely, this interaction has been demonstrated to enhance stability in areas protected by headland-induced wave shadowing. (Figures 16 and 17).

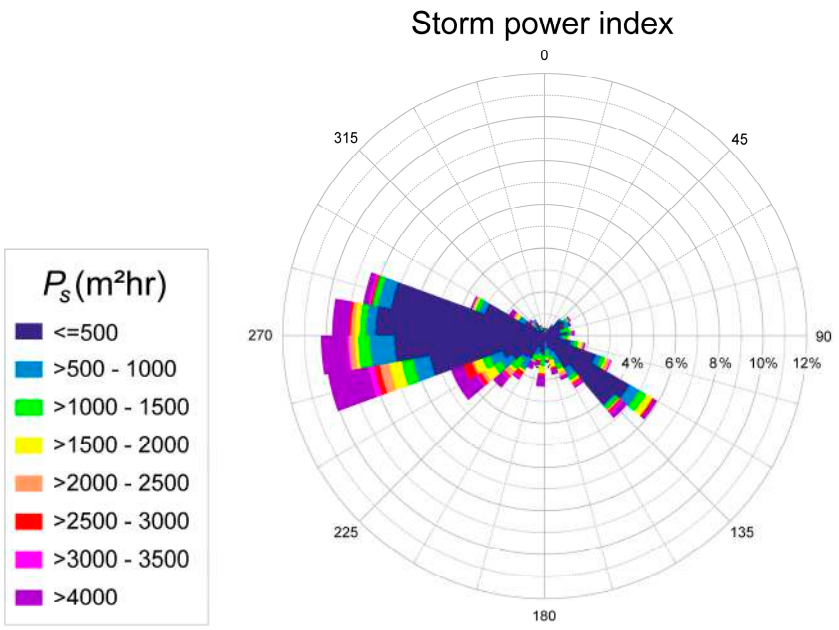

Figure 16. Storm power index and mean wave direction for the 1161 storm events computed by the POT method during the period between 1 January 1985 and 31 December 2022.

On the other hand, 158 storm events (equal to 13.6% of the total) approach with angles between 120° N and 150° N (Figure 16), with an average value of P_s equal to 606.2 m^2h. The maximum P_s values were computed for the event that occurred between March and April 2022 (14,265 m^2h) with a mean direction of 139° N, maximum H_s of 3.6 m and a duration of 1079 h.

However, various factors can influence shoreline evolution along the study area. Human activities, particularly the development of villages and tourist residences, have led to the deep modification of some dune systems located behind the beaches (see Appendix B). This is especially evident between beaches ID 65 (Cann'e Sisa) and ID 66 (Genn'e Mari), where a dune field was entirely occupied by residential buildings. Such urban development may have led to a sudden disruption in sediment transport between these adjacent dune-beach systems, potentially affecting the long-term evolution of the shoreline position.

The study analysed trends in shoreline variation at 79 beaches in southern Sardinia, representing the first survey of its kind conducted on the island over such a large area. The analysis identified the areas most affected by shoreline retreat.

The results show that the areas characterised by high shoreline variability are those subject to high anthropisation, primarily due to urban and industrial development rather than coastal protection structures. Buildings such as roads, piers, and ports may have altered natural processes, favouring shoreline retreat.

Furthermore, sector 3, the most anthropised zone of the study area, is also characterised by marked degradation of the *Posidonia oceanica* meadow. The health of the meadow and its upper limit can significantly influence coastal dynamics and contribute to the observed shoreline variation trends. This evidence is also relevant on a larger scale, in contexts where large-scale anthropogenic infrastructure, such as ports or other coastal works, affects the health of *Posidonia oceanica* meadows. The degradation of these meadows may affect coastal processes and result in shoreline retreat.

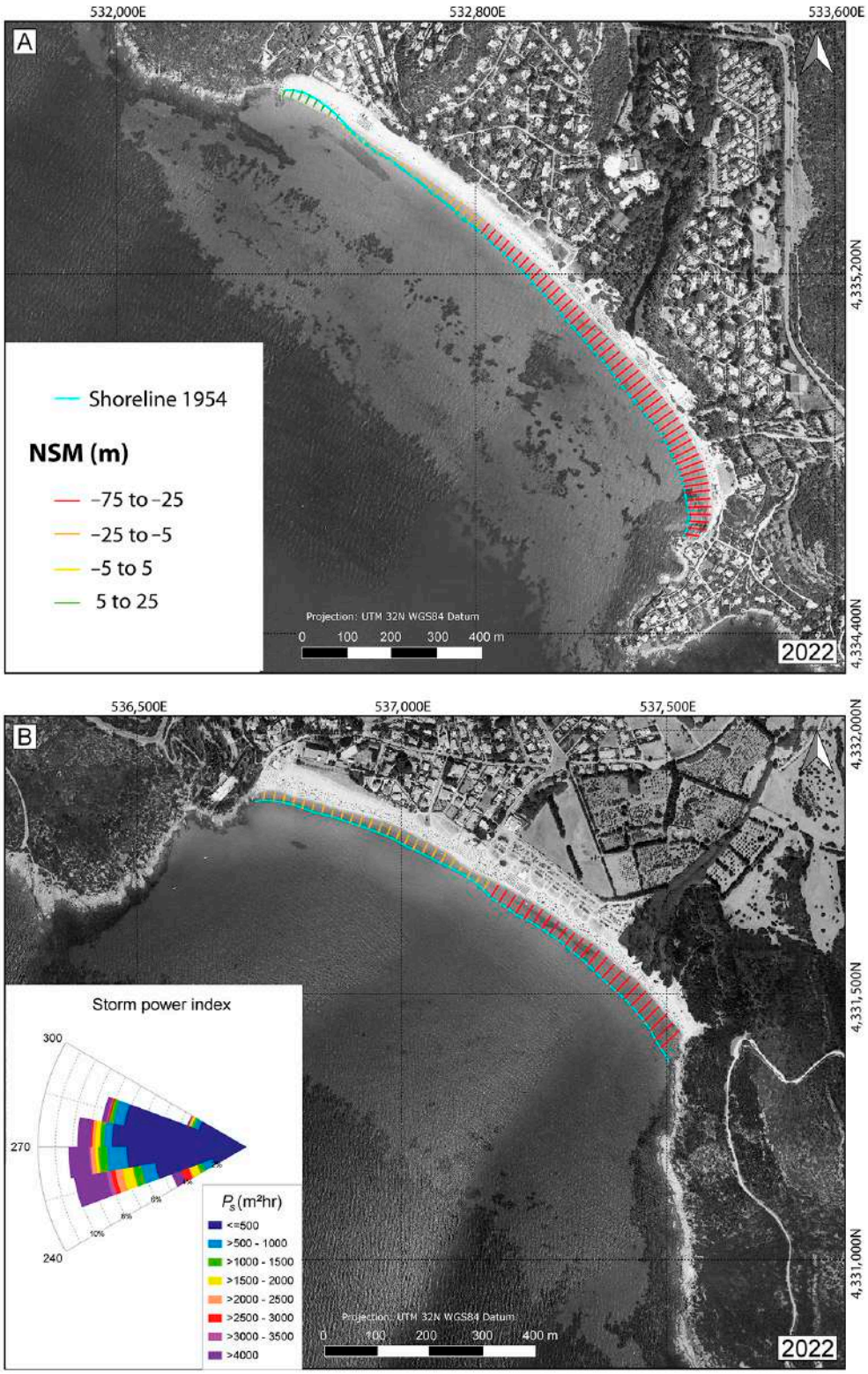

Figure 17. Panels (**A**,**B**) show Beach ID 64 (Kal'e Moru beach) and ID 68 (Solanas beach), respectively. Due to the prevailing wave regime (storm power index) and the partial protection provided by headlands, the south-eastern sectors of these beaches are subject to more intense processes of retreat compared to the north-western sectors, which tend to remain more stable or experience less pronounced retreat. This is highlighted by the NSM values in these beaches (coloured transects in panels (**A**,**B**)). The blue line represents the shoreline digitised from 1954 aerial orthophotos. Coordinate system: UTM 32N; Datum: WGS84.

Therefore, the study suggests that, when planning any coastal intervention, priority should be given to safeguarding and maintaining the health of *Posidonia oceanica*, as well as taking care to prevent infrastructure from interfering with the dynamics and resilience of the coastal system. This is particularly important in areas where the meadow is well developed, and the upper limit is close to the coastline.

4. Conclusions

This study provides a comprehensive assessment of long-term shoreline change trends along the southern coast of Sardinia by applying the Digital Shoreline Analysis System (DSAS) to a time series of aerial orthophotos spanning from 1954 to 2022. The results highlight the strong spatial variability of shoreline dynamics within a relatively long coastal stretch, reflecting the combined effects of natural factors, local morphology, wave climate, and anthropogenic modifications.

A key finding is the clear difference in behaviour between largely natural beaches and heavily urbanised, engineered coastal areas. Beaches with minimal human impact tend to be more resilient to natural shoreline movements; in fact, the balance between natural coastal processes and protective features such as dunes and headlands helps to mitigate the effects of storms and pressures from climate change, including sea level rise.

In contrast, beaches located near urban centres, harbours, or protected by rigid coastal structures, such as groynes and breakwaters, show the highest rates of shoreline retreat in the entire study area. These interventions, while often intended to defend specific assets or infrastructure, frequently disrupt natural longshore sediment transport, creating downdrift erosion hotspots and triggering unintended shoreline retreat. Similarly, the documented nourishment at Poetto beach has shown how artificial sediment input can temporarily modify beach morphology but often fails to deliver long-term stability when not adequately integrated into the local morphodynamic context. These examples all demonstrate that, if poorly planned, even nature-based engineering can have more negative than positive effects on shoreline stability.

Overall, these findings emphasise the critical importance of preserving and enhancing the natural resilience of coastal systems. Essential actions to minimise shoreline retreat risks and adapt effectively to future climate change scenarios include safeguarding natural sediment sources, maintaining functional dune systems, ensuring the ecological integrity of *Posidonia oceanica* meadows and carefully considering local wave exposure and sediment transport pathways. Conversely, where coastal modification is unavoidable, management strategies must be based on robust, site-specific data and an understanding of coastal processes to avoid repeating interventions that have caused more negative impacts than benefits.

This work demonstrates how combining detailed historical shoreline analysis with an understanding of local morphodynamics provides a valuable basis for supporting more adaptive and sustainable coastal management strategies, both for Sardinia and for other microtidal Mediterranean coastal stretches facing similar challenges.

Author Contributions: Conceptualisation, D.T. and S.S.; methodology, A.U. and S.S.; software, A.U., D.T., M.P. and S.S.; formal analysis, A.U., D.T. and S.S.; investigation, A.U., D.T. and S.S.; data curation, A.U., D.T., M.P., S.D. and S.S.; writing—original draft preparation, D.T., A.U. and S.S.; writing—review and editing, D.T., A.U., M.P., S.D. and S.S.; supervision, A.U., D.T. and S.S.; funding acquisition, S.D. All authors have read and agreed to the published version of the manuscript.

Funding: This research received no external funding.

Data Availability Statement: Data will be made available on request.

Acknowledgments: (A.U.) This publication was produced while attending the PhD programme in INNOVATION SCIENCES AND TECHNOLOGIES at the University of Cagliari, Cycle XXXVIII, with the support of a scholarship financed by the Ministerial Decree no. 351 of 9 April 2022, based on the NRRP—funded by the European Union—NextGenerationEU—Mission 4 "Education and Research", Component 1 "Enhancement of the offer of educational services: from nurseries to universities"—Investment 3.4 "Advanced teaching and university skills". (D.T.) This study was carried out within the RETURN Extended Partnership and received funding from the European Union Next-GenerationEU (National Recovery and Resilience Plan–NRRP, Mission 4, Component 2, Investment 1.3–D.D. 1243 2/8/2022, PE0000005). The research has also been funded by Regione Autonoma Sardegna under L.R. 7/2007, "Promozione della ricerca scientifica e dell'innovazione tecnologica in Sardegna" for BEACH and TENDER NEPTUNE projects, directed by Sandro DeMuro, University of Cagliari. The authors would like to thank the PROVIDUNE project (LIFE07NAT/IT/000519) for providing the coastal videomonitoring images. The authors would like to thank the "Mediterranean Geomorphological Coastal and Marine Laboratory" (MEDCOASTLAB), directed by Sandro DeMuro, Department of Chemical and Geological Sciences, University of Cagliari. (S.S.) This research was developed in the framework of Project "AMMIRARE" cofinanced by E.U. INTERREG P.O. Marittimo Italia Francia 2012–2027.

Conflicts of Interest: The authors declare that they have no known competing financial interests or personal relationships that could have appeared to influence the work reported in this paper.

Appendix A

Table A1. Statistical indicator values in Sector 1 (Shoreline Change Envelope—SCE; Net Shoreline Movement—NSM; End Point Rate—EPR; Weighted Linear Regression—WLR) calculated using the DSAS method for each beach identified along the studied coastal stretch. The table reports the mean, minimum, and maximum values of the statistical indicators, as well as the number of transects analysed for each beach.

Beach ID (n° tr.)	SCE		NSM		EPR		WLR	
	Mean	Min. | Max.	Mean	Min. | Max.	Mean	Min. | Max.	Mean	Min. | Max.
1 (21)	12.8	5.9 | 15.4	−2.1	−5.1 | 2.3	−0.03	−0.07 | 0.03	−0.07	−0.14 | 0.01
2 (47)	12.6	6.3 | 22.7	−6.0	−15.6 | –	−0.09	−0.23 | –	−0.11	−0.21 | 0.05
3 (12)	31.3	27.3 | 39.0	−8.4	−11.4 | –	−0.12	−0.17 | –	−0.27	−0.36 | –
4 (11)	14.1	6.8 | 17.2	−8.6	−12.2 | –	−0.13	−0.18 | –	−0.12	−0.18 | –
5 (5)	6.2	3.9 | 10.4	−1.2	−2.1 | –	−0.02	−0.03 | –	−0.07	−0.10 | –
6 (24)	13.8	4.0 | 25.0	1.0	−2.4 | 5.5	0.01	−0.06 | 0.08	−0.05	−0.08 | –
7 (7)	6.0	4.4 | 10.7	2.5	−1.6 | 10.7	0.04	−0.02 | 0.16	−0.01	−0.05 | 0.08
8 (10)	4.7	3.3 | 8.0	−3.3	−5.9 | –	−0.05	−0.09 | –	−0.06	−0.10 | –
9 (8)	11.5	5.9 | 15.2	−6.2	−8.3 | –	−0.09	−0.12 | –	−0.13	−0.17 | –
10 (2)	4.7	3.9 | 5.5	−0.9	−1.7 | –	−0.01	−0.02 | –	−0.03	−0.04 | –
11 (16)	25.9	5.3 | 34.1	−5–5.2	−12.1 | 3.4	−0.08	−0.18 | 0.05	−0.11	−0.19 | 0.01
12 (2)	8.5	7.9 | 9.0	−1.3	−1.6 | –	−0.02	−0.02 | –	−0.06	−0.06 | –
13 (3)	6.3	4.5 | 8.0	−3.3	−4.9 | –	−0.05	−0.07 | –	−0.07	−0.09 | –
14 (1)	6.1	6.1 | 6.1	−2.4	−2.4 | –	−0.03	−0.03 | –	−0.06	−0.06 | –
15 (2)	4.3	3.8 | 4.7	−1.1	−1.1 | –	−0.02	−0.02 | –	−0.03	−0.04 | –
16 (18)	12.6	5.0 | 19.1	−10.4	−18.3 | 1.7	−0.15	−0.27 | 0.02	−0.14	−0.27 | 0.01
17 (21)	18.5	6.6 | 28.9	2.7	−6.7 | 16.5	0.04	−0.10 | 0.24	−0.04	−0.09 | 0.01
18 (4)	3.7	1.8 | 5.6	−1.3	−2.0 | –	−0.02	−0.03 | –	−0.01	−0.03 | 0.02
19 (10)	7.0	1.9 | 14.2	−0.9	−3.7 | 0.5	−0.03	−0.21 | 0.01	−0.04	−0.11 | 0.03
20 (3)	11.3	9.6 | 13.2	0.7	– | 1.4	0.01	– | 0.02	−0.02	−0.04 | 0.01
21 (2)	3.6	2.9 | 4.3	−2.1	−3.0 | 0.9	−0.02	−0.04 | 0.01	−0.02	−0.04 | –
22 (3)	5.1	3.8 | 6.2	−6.0	−4.2 | 19.2	−0.04	−0.06 | –	−0.04	−0.06 | –

Table A2. Statistical indicator values in Sector 2 (Shoreline Change Envelope—SCE; Net Shoreline Movement—NSM; End Point Rate—EPR; Weighted Linear Regression—WLR) calculated using the DSAS method for each beach identified along the studied coastal stretch. The table reports the mean, minimum, and maximum values of the statistical indicators, as well as the number of transects analysed for each beach.

Beach ID (n° tr.)	SCE		NSM		EPR		WLR	
	Mean	Min. | Max.	Mean	Min. | Max.	Mean	Min. | Max.	Mean	Min. | Max.
23 (6)	29.2	26.0 | 32.0	0.9	−7.8 | 19.2	0.02	−0.12 | 0.32	0.02	−0.12 | 0.33
24 (65)	50.8	34.3 | 68.0	7.3	−6.8 | 32.0	0.11	−0.10 | 0.47	−0.01	−0.25 | 0.31
25 (24)	22.6	3.5 | 34.9	5.9	−0.7 | 13.2	0.09	−0.01 | 0.19	−0.03	−0.13 | 0.05
26 (2)	16.8	14.5 | 19.2	9.0	− | 9.9	0.13	− | 0.15	0.02	− | 0.03
27 (40)	22.2	7.6 | 38.8	3.4	− | 8.9	0.05	−0.06 | 0.30	−0.03	−0.09 | 0.08
28 (15)	9.4	2.9 | 27.4	−0.7	−8.7 | 8.1	−0.01	−0.13 | 0.12	−0.04	−0.15 | 0.01
29 (2)	15.5	14.7 | 16.4	4.1	−1.4 | 9.6	0.07	−0.02 | 0.16	0.18	− | 0.21
30 (16)	22.0	5.0 | 38.8	−6.9	−26.2 | 5.2	−0.07	−0.38 | 0.40	−0.10	−0.43 | 0.35
31 (143)	20.5	2.5 | 35.4	−1.0	−15.7 | 14.0	−0.02	−0.68 | 0.22	−0.04	−0.64 | 0.26
32 (56)	13.2	5.6 | 32.2	−4.0	−11.3 | 4.1	−0.06	−0.17 | 0.06	−0.10	−0.30 | 0.01
33 (16)	5.0	3.4 | 7.7	1.7	−2.9 | 5.4	0.02	−0.06 | 0.08	−0.02	−0.08 | 0.04
34 (14)	7.4	4.6 | 11.6	−6.6	−11.6 | −	−0.10	−0.17 | −	−0.08	−0.11 | −
35 (9)	11.3	8.7 | 14.5	−8.3	−11.6 | −	−0.12	−0.17 | −	−0.10	−0.16 | −
36 (28)	11.2	4.1 | 17.4	−6.5	−13.3 | −	−0.10	−0.20 | −	−0.09	−0.18 | −
37 (125)	12.0	2.6 | 22.4	−2.9	−12.3 | 5.6	−0.04	−0.18 | 0.08	−0.01	−0.18 | 0.14
38 (59)	16.6	9.9 | 26.4	−9.5	−17.9 | 9.4	−0.14	−0.28 | 0.14	−0.14	−0.35 | 0.38
39 (73)	9.5	3.3 | 16.5	−2.0	−9.8 | 5.5	−0.03	−0.39 | 0.08	−0.03	−0.43 | 0.06
40 (83)	14.5	4.0 | 45.0	3.8	−8.4 | 28.6	0.06	−0.12 | 0.42	0.01	−0.11 | 0.37
41 (83)	28.8	4.9 | 68.8	−18.2	−46.2 | 57.4	−0.30	−1.25 | 0.84	−0.15	−1.22 | 1.19

Table A3. Statistical indicator values in Sector 3 (Shoreline Change Envelope—SCE; Net Shoreline Movement—NSM; End Point Rate—EPR; Weighted Linear Regression—WLR) calculated using the DSAS method for each beach identified along the studied coastal stretch. The table reports the mean, minimum, and maximum values of the statistical indicators, as well as the number of transects analysed for each beach.

Beach ID (n° tr.)	SCE		NSM		EPR		WLR	
	Mean	Min. | Max.	Mean	Min. | Max.	Mean	Min. | Max.	Mean	Min. | Max.
42 (13)	27.3	19.2 | 35.7	−13.5	−23.7 | −	−0.20	−0.35 | −	−0.08	−0.34 | 0.12
43 (11)	79.6	56.0 | 94.8	−61.3	−94.1 | −	−0.96	−1.42 | −	−0.78	−1.23 | −
44 (6)	97.1	87.9 | 105.1	−87.8	−96.1 | −	−1.44	−1.56 | −	−1.32	−1.46 | −
45 (4)	64.7	53.4 | 79.3	−58.5	−79.3 | −	−0.87	−1.22 | −	−0.70	−0.99 | −
46 (68)	34.6	13.6 | 85.1	−16.1	−84.7 | 22.1	−0.24	−1.24 | 0.32	−0.13	−0.77 | 0.34
47 (8)	116.3	106.2 | 135.4	−114.8	−132.2 | −	−1.69	−1.94 | −	−1.45	−1.59 | −
48 (61)	30.0	12.7 | 41.8	7.2	−11.2 | 19.0	0.10	−0.25 | 0.28	−0.09	−0.47 | 0.23
49 (4)	26.8	23.4 | 31.3	4.4	− | 9.3	0.06	− | 0.14	0.11	− | 0.16
50 (34)	34.6	19.9 | 54.0	26.5	−6.2 | 54.0	0.39	−0.09 | 0.79	0.35	−0.16 | 0.88
51 (149)	41.6	19.6 | 75.7	3.4	−32.8 | 73.3	0.05	−0.48 | 1.08	−0.02	−0.74 | 1.27
52 (58)	48.5	29.8 | 93.4	44.1	− | 90.8	0.65	− | 1.33	0.66	− | 1.36
53 (3)	7.1	4.3 | 9.7	−3.8	−5.5 | −	−0.08	−0.12 | −	−0.06	−0.12 | −
54 (7)	6.2	3.3 | 7.9	−0.2	−7.9 | 4.6	−0.02	−0.18 | 0.10	0.03	−0.18 | 0.12
55 (401)	33.1	6.8 | 84.8	10.2	−18.3 | 83.6	0.15	−0.27 | 1.23	0.17	−0.43 | 0.86

Table A4. Statistical indicator values in Sector 4 (Shoreline Change Envelope—SCE; Net Shoreline Movement—NSM; End Point Rate—EPR; Weighted Linear Regression—WLR) calculated using the DSAS method for each beach identified along the studied coastal stretch. The table reports the mean, minimum, and maximum values of the statistical indicators, as well as the number of transects analysed for each beach.

Beach ID (n° tr.)	SCE		NSM		EPR		WLR	
	Mean	Min. | Max.	Mean	Min. | Max.	Mean	Min. | Max.	Mean	Min. | Max.
56 (119)	14.0	6.7 | 32.8	−3.2	−15.8 | 8.5	−0.05	−0.23 | 0.12	−0.05	−0.25 | 0.09
57 (21)	15.2	6.6 | 44.6	−6.6	−16.5 | 24.7	−0.21	−0.59 | 0.36	−0.14	−0.56 | 0.60
58 (42)	6.8	0.7 | 12.5	−4.4	−12.5 | 2.6	−0.06	−0.18 | 0.06	−0.06	−0.22 | 0.09
59 (18)	7.5	1.6 | 20.0	−4.7	−13.4 | 4.3	−0.07	−0.20 | 0.06	−0.07	−0.19 | 0.14
60 (17)	6.5	3.0 | 11.0	−4.7	−8.5 | –	−0.07	−0.13 | –	−0.03	−0.08 | 0.01
61 (6)	3.8	3.5 | 4.3	−0.4	−1.6 | 0.6	−0.01	−0.02 | 0.01	−0.03	−0.04 | –
62 (19)	6.3	4.0 | 11.4	3.0	−0.4 | 8.0	0.04	−0.01 | 0.12	−0.02	−0.09 | 0.05
63 (13)	4.9	2.9 | 6.0	−1.0	−4.9 | 4.2	−0.01	−0.07 | 0.06	0.01	−0.05 | 0.05
64 (76)	41.2	24.7 | 55.9	−28.8	−55.9 | 19.9	−0.42	−0.82 | 0.29	−0.12	−0.52 | 0.22
65 (21)	31.4	21.8 | 47.3	−28.4	−46.6 | –	−0.42	−0.75 | –	−0.21	−0.35 | –
66 (27)	19.2	10.2 | 24.6	−16.0	−21.0 | –	−0.24	−0.31 | –	−0.11	−0.18 | –
67 (7)	4.8	4.2 | 5.1	−1.5	−2.0 | –	−0.02	−0.03 | –	−0.03	−0.05 | –
68 (49)	33.3	19.3 | 47.0	−25.0	−47.0 | –	−0.37	−0.69 | –	−0.17	−0.33 | –
69 (35)	12.3	7.2 | 20.2	−2.9	−9.8 | 3.4	−0.04	−0.14 | 0.05	−0.06	−0.19 | 0.06
70 (10)	11.0	6.5 | 16.1	−7.3	−14.7 | –	−0.11	−0.22 | –	−0.12	−0.16 | –
71 (9)	17.7	8.7 | 21.5	1.1	– | 2.2	0.02	– | 0.03	−0.07	−0.14 | –
72 (39)	15.3	3.5 | 25.7	3.3	−7.9 | 16.4	0.05	−0.12 | 0.24	0.01	−0.08 | 0.19
73 (11)	14.4	5.4 | 21.0	−1.3	−6.1 | 3.2	−0.02	−0.09 | 0.05	−0.13	−0.15 | –
74 (55)	9.3	2.6 | 19.9	−4.5	– | 2.6	−0.06	−0.22 | 0.19	−0.08	−0.27 | 0.03
75 (24)	23.1	2.1 | 119.9	5.0	−33.7 | 108.1	0.01	−0.50 | 1.59	0.04	−0.73 | 1.94
76 (7)	4.0	2.3 | 7.2	−1.7	−6.9 | 1.2	−0.02	−0.10 | 0.02	−0.02	−0.04 | 0.01
77 (13)	6.1	3.4 | 9.1	1.4	−4.3 | 3.4	0.02	−0.08 | 0.05	−0.02	−0.07 | 0.01
78 (5)	7.2	4.9 | 9.6	−1.0	−2.1 | 1.0	−0.02	−0.03 | 0.01	−0.01	−0.06 | 0.03
79 (12)	9.1	4.3 | 13.8	−6.7	−13.6 | –	−0.10	−0.20 | –	−0.06	−0.13 | 0.02

Appendix B

Table A5. Main types of potential anthropogenic impacts on the studied beaches in Sector 1: (1) Impacts on dune systems; (2) Use of heavy vehicles for: removal of *Posidonia oceanica* banquettes during "beach cleaning" operations; military exercises; (3) Presence of infrastructures on the beach system: coastal engineering structures (e.g., breakwaters and more) and coastal defence operations (beach nourishment); artificial infrastructures (e.g., tourist infrastructures and buildings); (4) Artificial structures located landward from the beach system (e.g., dams and more); (5) Impacts on the upper limit of *Posidonia oceanica* meadow. The table includes the following indications: impact present (X), absent (A) or not defined (ND) (data from [87,88]); impact presumed present (PP), presumed absent (PA) or not defined (ND) (from the analysis of aerial orthophotos).

Beach ID	Impacts on Dune Systems	Transit of Heavy Vehicles on the Beach	Infrastructures on the Beach System		Artificial Structures Located Landward from the Beach	Impacts on *Posidonia oceanica* Meadow
			Coastal Engineering Structures/Coastal Defence Operations	Artificial Infrastructures		
1	PA	ND	PA	PA	ND	ND
2	X [87]	X [87]	A [87]	A [87]	ND	A [87]
3	X [87]	X [87]	A [87]	A [87]	ND	A [87]
4	PP	ND	PA	PA	ND	ND

Table A5. *Cont.*

Beach ID	Impacts on Dune Systems	Transit of Heavy Vehicles on the Beach	Infrastructures on the Beach System		Artificial Structures Located Landward from the Beach	Impacts on *Posidonia oceanica* Meadow
			Coastal Engineering Structures/Coastal Defence Operations	Artificial Infrastructures		
5	PP	ND	PA	PA	ND	ND
6	X [87]	ND	A [87]	X [87]	ND	A [87]
7	PP	X [88]	PP	PA	ND	ND
8	PP	ND	PA	PA	ND	ND
9	PP	ND	PA	PA	ND	ND
10	ND	ND	PA	PA	ND	ND
11	X [87]	ND	A [87]	X [87]	ND	A [87]
12	ND	ND	PA	PA	ND	ND
13	ND	ND	PA	PA	ND	ND
14	ND	ND	PA	PA	ND	ND
15	ND	ND	PA	PA	ND	ND
16	PP	X [88]	PA	PP	ND	ND
17	X [87]	ND	A [87]	X [87]	ND	A [87]
18	PP	ND	PA	PA	ND	ND
19	ND	ND	PA	PA	ND	ND
20	PP	ND	PA	PA	ND	ND
21	PA	ND	PA	PA	ND	ND
22	PP	ND	PA	PA	ND	ND

Table A6. Main types of potential anthropogenic impacts on the studied beaches in Sector 2: (1) Impacts on dune systems; (2) Use of heavy vehicles for: removal of *Posidonia oceanica* banquettes during "beach cleaning" operations; military exercises; (3) Presence of infrastructures on the beach system: coastal engineering structures (e.g., breakwaters and more) and coastal defence operations (beach nourishment); artificial infrastructures (e.g., tourist infrastructures and buildings); (4) Artificial structures located landward from the beach system (e.g., dams and more); (5) Impacts on the upper limit of *Posidonia oceanica* meadow. The table includes the following indications: impact present (X), absent (A) or not defined (ND) (data from [57,87,88]); impact presumed present (PP), presumed absent (PA) or not defined (ND) (from the analysis of aerial orthophotos).

Beach ID	Impacts on Dune Systems	Transit of Heavy Vehicles on the Beach	Infrastructures on the Beach System		Artificial Structures Located Landward from the Beach	Impacts on *Posidonia oceanica* Meadow
			Coastal Engineering Structures/Coastal Defence Operations	Artificial Infrastructures		
23	X [87]	ND	A [87]	A [87]	ND	A [87]
24	X [87]	ND	A [87]	X [87]	ND	A [87]
25	X [87]	ND	A [87]	X [87]	ND	A [87]
26	PP	ND	PA	PA	ND	ND
27	X [87]	ND	A [87]	X [87]	X [57]	A [87]
28	X [87]	ND	A [87]	X [87]	ND	A [87]
29	X [87]	X [88]	PA	PA	ND	A [87]
30	X [87]	X [88]	A [87]	X [87]	ND	A [87]
31	X [87]	X [88]	PA	X [87]	X [57]	A [87]

Table A6. *Cont.*

Beach ID	Impacts on Dune Systems	Transit of Heavy Vehicles on the Beach	Infrastructures on the Beach System		Artificial Structures Located Landward from the Beach	Impacts on *Posidonia oceanica* Meadow
			Coastal Engineering Structures/Coastal Defence Operations	Artificial Infrastructures		
32	ND [87]	X [88]	A [87]	X [87]	ND	A [87]
33	PP	ND	PA	PA	ND	ND
34	PP	ND	PA	PA	ND	ND
35	PP	ND	PA	PA	ND	ND
36	PP	ND	PA	PA	ND	ND
37	X [87]	X [88]	A [87]	X [87]	X [57]	ND [87]
38	X [87]	ND	PP	X [87]	ND	ND [87]
39	X [87]	X [88]	A [87]	X [87]	ND	A [87]
40	X [87]	ND	PP	X [87]	X [57]	ND [87]
41	X [87]	X [88]	X [87]	X [87]	ND	A [87]

Table A7. Main types of potential anthropogenic impacts on the studied beaches in Sector 3: (1) Impacts on dune systems; (2) Use of heavy vehicles for: removal of *Posidonia oceanica* banquettes during "beach cleaning" operations; military exercises; (3) Presence of infrastructures on the beach system: coastal engineering structures (e.g., breakwaters and more) and coastal defence operations (beach nourishment); artificial infrastructures (e.g., tourist infrastructures and buildings); (4) Artificial structures located landward from the beach system (e.g., dams and more); (5) Impacts on the upper limit of *Posidonia oceanica* meadow. The table includes the following indications: impact present (X), absent (A) or not defined (ND) (data from [57,60,84,87,88]); impact presumed present (PP), presumed absent (PA) or not defined (ND) (from the analysis of aerial orthophotos).

Beach ID	Impacts on Dune Systems	Transit of Heavy Vehicles on the Beach	Infrastructures on the Beach System		Artificial Structures Located Landward from the Beach	Impacts on *Posidonia oceanica* Meadow
			Coastal Engineering Structures/Coastal Defence Operations	Artificial Infrastructures		
42	X [87]	ND	X [87]	X [87]	X [57]	X [84,87]
43	X [87]	ND	X [87]	X [87]	ND	X [84,87]
44	X [87]	ND	X [87]	X [87]	ND	X [84,87]
45	X [87]	ND	X [87]	X [87]	ND	X [84,87]
46	X [87]	X [88]	X [87]	X [87]	ND	X [84,87]
47	X [87]	X [88]	X [87]	X [87]	ND	X [84,87]
57	X [87]	ND	X [87]	X [87]	X [57]	X [84,87]
49	X [87]	ND	X [87]	X [87]	ND	X [84,87]
50	X [87]	ND	X [87]	X [87]	X [57]	X [84,87]
51	X [87]	ND	X [87]	X [87]	X [57]	X [84,87]
52	X [87]	ND	X [87]	X [87]	ND	X [84,87]
53	PP	ND	PP	PP	ND	ND
54	ND [87]	ND	A [87]	X [87]	ND	A [87]
55	X [87]	X [60,88]	X [87]	X [87]	X [57]	X [84,87]

Table A8. Main types of potential anthropogenic impacts on the studied beaches in Sector 4: (1) Impacts on dune systems; (2) Use of heavy vehicles for: removal of *Posidonia oceanica* banquettes during "beach cleaning" operations; military exercises; (3) Presence of infrastructures on the beach system: coastal engineering structures (e.g., breakwaters and more) and coastal defence operations (beach nourishment); artificial infrastructures (e.g., tourist infrastructures and buildings); (4) Artificial structures located landward from the beach system (e.g., dams and more); (5) Impacts on the upper limit of *Posidonia oceanica* meadow. The table includes the following indications: impact present (X), absent (A) or not defined (ND) (data from [57,87,88]); impact presumed present (PP), presumed absent (PA) or not defined (ND) (from the analysis of aerial orthophotos).

Beach ID	Impacts on Dune Systems	Transit of Heavy Vehicles on the Beach	Infrastructures on the Beach System		Artificial Structures Located Landward from the Beach	Impacts on *Posidonia oceanica* Meadow
			Coastal Engineering Structures/Coastal Defence Operations	Artificial Infrastructures		
56	PP	ND	PP	PP	X [57]	ND
57	PP	ND	PP	PP	ND	ND
58	ND	ND	PA	PP	X [57]	ND
59	ND	ND	PP	PP	ND	ND
60	PP	ND	PA	PP	ND	ND
61	X [87]	ND	A [87]	PA	ND	A [87]
62	X [87]	ND	A [87]	X [87]	ND	A [87]
63	X [87]	ND	A [87]	X [87]	ND	A [87]
64	X [87]	X [88]	A [87]	X [87]	ND	A [87]
65	X [87]	X [88]	A [87]	X [87]	ND	ND [87]
66	X [87]	ND	A [87]	X [87]	ND	A [87]
67	ND	ND	PA	PA	ND	ND
68	X [87]	ND	A [87]	X [87]	ND	A [87]
69	X [87]	ND	A [87]	X [87]	ND	A [87]
70	X [87]	X [88]	A [87]	X [87]	ND	ND [87]
71	PP	ND	PA	PA	ND	ND
72	X [87]	ND	A [87]	X [87]	ND	X [87]
73	PA	ND	PA	PP	ND	ND
74	X [87]	X [88]	A [87]	X [87]	ND	ND [87]
75	X [87]	ND	X [87]	X [87]	ND	ND [87]
76	PP	ND	PP	PA	ND	ND
77	PP	ND	PA	PP	ND	ND
78	PP	ND	PA	PP	ND	ND
79	PP	ND	PA	PP	ND	ND

References

1. Green, D.; Woodroffe, C.; Evelpidou, N.; Delgado-Fernandez, I.; Karkani, A.; Ciavola, P. Coastal systems: The dynamic interface between land and sea. In *Research Directions, Challenges and Achievements of Modern Geography*, 1st ed.; Bański, J., Meadows, M., Eds.; Advances in Geographical and Environmental Sciences (AGES); Springer: Singapore, 2023; pp. 207–229. [CrossRef]
2. Vousdoukas, M.I.; Ranasinghe, R.; Mentaschi, L.; Plomaritis, T.A.; Athanasiou, P.; Luijendijk, A.; Feyen, L. Sandy coastlines under threat of erosion. *Nat. Clim. Chang.* **2020**, *10*, 260–263. [CrossRef]
3. Luijendijk, A.; Hagenaars, G.; Ranasinghe, R.; Baart, F.; Donchyts, G.; Aarninkhof, S. The State of the World's Beaches. *Sci. Rep.* **2018**, *8*, 6641. [CrossRef]
4. Hemer, M.; Fan, Y.; Mori, N. Projected changes in wave climate from a multi-model ensemble. *Nat. Clim. Chang.* **2013**, *3*, 471–476. [CrossRef]
5. Schroeder, K.; Chiggiato, J.; Josey, S.A.; Borghini, M.; Aracri, S.; Sparnocchia, S. Rapid response to climate change in a marginal sea. *Sci. Rep.* **2017**, *7*, 4065. [CrossRef]
6. Chefaoui, R.M.; Duarte, C.M.; Serrão, E.A. Dramatic loss of seagrass habitat under projected climate change in the Mediterranean Sea. *Glob. Change Biol.* **2018**, *24*, 4919–4928. [CrossRef]
7. Casas-Prat, M.; Sierra, J.P. Projected future wave climate in the NW Mediterranean Sea. *J. Geophys. Res. Oceans* **2013**, *118*, 3548–3568. [CrossRef]

8. Lionello, P.; Bhend, J.; Buzzi, A.; Della-Marta, P.M.; Krichak, S.O.; Jansà, A.; Maheras, P.; Sanna, A.; Trigo, I.F.; Trigo, R. Chapter 6 Cyclones in the Mediterranean region: Climatology and effects on the environment. *Dev. Earth Environ. Sci.* **2006**, *4*, 325–372.
9. Nissen, K.M.; Leckebusch, G.C.; Pinto, J.G.; Ulbrich, U. Mediterranean cyclones and windstorms in a changing climate. *Reg. Environ. Chang.* **2010**, *10*, 19–32. [CrossRef]
10. Knutson, T.; Camargo, S.; Chan, J.; Emanuel, K.; Ho, C.; Kossin, J.; Mohapatra, M.; Satoh, M.; Sugi, M.; Walsh, K.; et al. Tropical cyclones and climate change assessment: Part II. Projected response to anthropogenic warming. *Bull. Am. Meteorol. Soc.* **2020**, *101*, E202–E322. [CrossRef]
11. Lira-Loarca, A.; Besio, G. Future changes and seasonal variability of the directional wave spectra in the Mediterranean Sea for the 21st century. *Environ. Res. Lett.* **2020**, *17*, 104015. [CrossRef]
12. Pérez Gómez, B.; Vilibić, I.; Šepić, J.; Međugorac, I.; Ličer, M.; Testut, L.; Fraboul, C.; Marcos, M.; Abdellaoui, H.; Álvarez Fanjul, E.; et al. Coastal sea level monitoring in the Mediterranean and Black seas. *Ocean Sci.* **2022**, *18*, 997–1053. [CrossRef]
13. Meli, M.; Camargo, C.M.L.; Olivieri, M.; Slangen, A.B.A.; Romagnoli, C. Sea-level trend variability in the Mediterranean during the 1993–2019 period. *Front. Mar. Sci.* **2023**, *10*, 1150488. [CrossRef]
14. Dieng, H.B.; Cazenave, A.; Gouzenes, Y.; Sow, B.A. Trends and inter-annual variability of altimetry-based coastal sea level in the Mediterranean Sea: Comparison with tide gauges and models. *Adv. Space Res.* **2021**, *68*, 3279–3290. [CrossRef]
15. Sarkar, N.; Rizzo, A.; Vandelli, V.; Soldati, M. A literature review of climate-related coastal risks in the Mediterranean, a climate change hotspot. *Sustainability* **2022**, *14*, 15994. [CrossRef]
16. Duarte, C.M. Seagrass depth limits. *Aquat. Bot.* **1991**, *40*, 363–377. [CrossRef]
17. Gobert, S.; Cambridge, M.; Velimirov, B.; Pergent, G.; Lepoint, G.; Bouquegneau, J.-M.; Dauby, P.; Pergent-Martini, C.; Walker, D.; Larkum, A.; et al. Biology of Posidonia. In *Seagrasses: Biology, Ecology and Conservation*; Springer: Dordrecht, The Netherlands, 2006; pp. 387–408. [CrossRef]
18. Armenio, E.; De Serio, F.; Mossa, M.; Petrillo, A.F. Coastline evolution based on statistical analysis and modeling. *Nat. Hazards Earth Syst. Sci.* **2019**, *19*, 1937–1953. [CrossRef]
19. Feyssat, P.; Certain, R.; Robin, N.; Barusseau, J.P.; Lamy, A.; Raynal, O.; Hebert, B. Morphodynamics of two Mediterranean microtidal beaches presenting permanent megacusps under the influence of waves and strong offshore winds. *Cont. Shelf Res.* **2024**, *272*, 105160. [CrossRef]
20. Bowman, D.; Guillén, J.; López, L.; Pellegrino, V. Planview geometry and morphological characteristics of pocket beaches on the Catalan coast (Spain). *Geomorphology* **2009**, *108*, 191–199. [CrossRef]
21. Short, A.D.; Masselink, G. Embayed and structurally controlled beaches. In *Handbook of Beach and Shoreface Morphodynamics*; Short, A.D., Ed.; John Wiley and Sons: Chichester, UK, 1999; pp. 230–250.
22. Gallop, S.L.; Kennedy, D.M.; Loureiro, C.; Naylor, L.A.; Muñoz-Pérez, J.J.; Jackson, D.W.T.; Fellowes, T.E. Geologically controlled sandy beaches: Their geomorphology, morphodynamics and classification. *Sci. Total Environ.* **2020**, *731*, 139123. [CrossRef] [PubMed]
23. Ruessink, G.; Ranasinghe, R. Beaches. In *Coastal Environments and Global Change*; Masselink, G., Gehrels, R., Eds.; John Wiley and Sons: Chichester, UK, 2015; pp. 149–177. [CrossRef]
24. Celata, F.; Gioia, E. Resist or retreat? Beach erosion and the climate crisis in Italy: Scenarios, impacts and challenges. *Appl. Geog.* **2024**, *169*, 103335. [CrossRef]
25. Le Cozannet, G.; Rohmer, J.; Cazenave, A.; Idier, D.; Van De Wal, R.; De Winter, R.; Pedreros, R.; Balouin, Y.; Vinchon, C.; Oliveros, C. Evaluating uncertainties of future marine flooding occurrence as sea-level rises. *Environ. Model. Softw.* **2015**, *73*, 44–56. [CrossRef]
26. Ginesu, S.; Carboni, D.; Marian, M. Coastline modifications in Sardinia starting from archaeological data: A progress report. *Procedia Environ. Sci.* **2012**, *14*, 132–142. [CrossRef]
27. Marriner, N.; Morhange, C.; Goiran, J.P. Coastal and ancient harbour geoarchaeology. *Geol. Today* **2010**, *26*, 21–27. [CrossRef]
28. Porta, M.; Buosi, C.; Trogu, D.; Ibba, A.; De Muro, S. An integrated sea-land approach for analyzing forms, processes, deposits and the evolution of the urban coastal belt of Cagliari. *J. Maps* **2021**, *17*, 65–74. [CrossRef]
29. Foti, G.; Barbaro, G.; Barillà, G.C.; Mancuso, P. Shoreline changes due to the construction of ports: Case study—Calabria (Italy). *J. Mar. Sci. Eng.* **2023**, *11*, 2382. [CrossRef]
30. De Falco, G.; Simeone, S.; Baroli, M. Management of beach-cast *Posidonia oceanica* seagrass on the Island of Sardinia (Italy, Western Mediterranean). *J. Coast. Res.* **2008**, *24*, 69–75. [CrossRef]
31. Dentamare, I.; Capasso, L.; Chianese, E.; Calicchio, R.; Franzese, P.P.; Grande, U.; Russo, G.F.; Buonocore, E. Ecological implications of *Posidonia oceanica* banquette removal: Potential loss of natural capital and ecosystem services. *Water* **2025**, *17*, 1362. [CrossRef]
32. Astier, J.M.; Boudouresque, C.; Pergent, G.; Pergent-Martini, C. Non-removal of the *Posidonia oceanica* "banquette" on a beach very popular with tourists: Lessons from Tunisia. *Sci. Rep. Port-Cros Natl. Park* **2020**, *34*, 15–21.
33. Simeone, S.; Palombo, L.; Molinaroli, E.; Brambilla, W.; Conforti, A.; De Falco, G. Shoreline response to wave forcing and sea level rise along a geomorphological complex coastline (Western Sardinia, Mediterranean Sea). *Appl. Sci.* **2021**, *11*, 4009. [CrossRef]

34. Boudouresque, C.F.; Ponel, P.; Astruch, P.; Barcelo, A.; Blanfuné, A.; Geoffroy, D.; Thibaut, T. The high heritage value of the Mediterranean sandy beaches, with a particular focus on the *Posidonia oceanica* "banquettes": A review. *Sci. Rep. Port-Cros Natl. Park* **2017**, *31*, 23–70.
35. Trogu, D.; Simeone, S.; Usai, A.; Porta, M.; De Muro, S. On the role of wood and seagrass rests in coastal flooding events in Mediterranean microtidal beaches. *J. Coast. Res.* **2024**, *113*, 115–119. [CrossRef]
36. Bitan, M.; Galili, E.; Spanier, E.; Zviely, D. Beach nourishment alternatives for mitigating erosion of ancient coastal sites on the Mediterranean Coast of Israel. *J. Mar. Sci. Eng.* **2020**, *8*, 509. [CrossRef]
37. Costa, G.P.; Marino, M.; Cáceres, I.; Musumeci, R.E. Effectiveness of dune reconstruction and beach nourishment to mitigate coastal erosion of the Ebro Delta (Spain). *J. Mar. Sci. Eng.* **2023**, *11*, 1908. [CrossRef]
38. Pranzini, E. Il colore della sabbia: Percezione, caratterizzazione e compatibilità nel ripascimento artificiale delle spiagge. *Studi Costieri* **2008**, *15*, 89–108.
39. Cenci, L.; Disperati, L.; Persichillo, M.G.; Oliveira, E.R.; Alves, F.L.; Phillips, M. Integrating remote sensing and GIS techniques for monitoring and modeling shoreline evolution to support coastal risk management. *GISci. Remote Sens.* **2017**, *55*, 355–375. [CrossRef]
40. Kumar, B.S.; Balukkarasu, A.; Tamilarasan, K. Coastal vulnerability mapping using remote sensing and GIS techniques in Tuticorin Coast of Tamil Nadu, India. *J. Geogr. Environ. Earth Sci. Int.* **2019**, *20*, 1–12. [CrossRef]
41. Chawalit, C.; Boonpook, W.; Sitthi, A.; Torsri, K.; Kamthonkiat, D.; Tan, Y.; Suwansaard, A.; Nardkulpat, A. Geoinformatics and machine learning for shoreline change monitoring: A 35-year analysis of coastal erosion in the upper Gulf of Thailand. *ISPRS Int. J. Geo-Inf.* **2025**, *14*, 94. [CrossRef]
42. Sytnik, O.; Del Río, L.; Greggio, N.; Bonetti, J. Historical shoreline trend analysis and drivers of coastal change along the Ravenna coast, NE Adriatic. *Environ. Earth Sci.* **2018**, *77*, 779. [CrossRef]
43. Fernández-Hernández, M.; Calvo, A.; Iglesias, L.; Castedo, R.; Ortega, J.J.; Diaz-Honrubia, A.J.; Mora, P.; Costamagna, E. Anthropic Action on Historical Shoreline Changes and Future Estimates Using GIS: Guadarmar Del Segura (Spain). *Appl. Sci.* **2023**, *13*, 9792. [CrossRef]
44. Castedo, R.; de la Vega-Panizo, R.; Fernández-Hernández, M.; Paredes, C. Measurement of historical cliff-top changes and estimation of future trends using GIS data between Bridlington and Hornsea–Holderness Coast (UK). *Geomorphology* **2015**, *230*, 146–160. [CrossRef]
45. Islam, M.S.; Crawford, T.W. Assessment of Spatio-Temporal Empirical Forecasting Performance of Future Shoreline Positions. *Remote Sens.* **2022**, *14*, 6364. [CrossRef]
46. Franco-Ochoa, C.; Zambrano-Medina, Y.; Plata-Rocha, W.; Monjardín-Armenta, S.; Rodríguez-Cueto, Y.; Escudero, M.; Mendoza, E. Long-Term Analysis of Wave Climate and Shoreline Change along the Gulf of California. *Appl. Sci.* **2020**, *10*, 8719. [CrossRef]
47. Himmelstoss, E.A.; Henderson, R.E.; Kratzmann, M.G.; Farris, A.S. Digital Shoreline Analysis System (DSAS) version 5.1 user guide. In *U.S. Geological Survey Open-File Report*; No. 2021-1091; U.S. Geological Survey: Reston, VA, USA, 2021. [CrossRef]
48. Kuleli, T.; Guneroglu, A.; Karsli, F.; Dihkan, M. Automatic detection of shoreline change on coastal Ramsar wetlands of Turkey. *Ocean Eng.* **2011**, *38*, 1141–1149. [CrossRef]
49. Kaddour, S.; Hemdane, Y.; Kessali, N.; Belabdi, K.; Sallaye, M. Study of shoreline changes through Digital Shoreline Analysis System and wave modeling: Case of the sandy coast of Bou-Ismail Bay, Algeria. *Ocean Sci.* **2020**, *57*, 493–527. [CrossRef]
50. Pepe, M.; Costantino, D.; Alfio, V.S. A GIS procedure to assess shoreline changes over time using multi-temporal maps: An analysis of a sandy shoreline in Southern Italy over the last 100 years. *Geomat. Environ. Eng.* **2023**, *17*, 107–134. [CrossRef]
51. Laksono, F.A.T.; Borzì, L.; Distefano, S.; Czirok, L.; Halmai, Á.; Di Stefano, A. Shoreline change dynamics along the Augusta Coast, Eastern Sicily, South Italy. *Earth Surf. Process. Landf.* **2023**, *48*, 2630–2641. [CrossRef]
52. Usai, A.; Simeone, S.; Trogu, D.; Porta, M.; De Muro, S. Morphometric analysis and classification of the embayed beaches on the southern coast of Sardinia Island (Western Mediterranean Sea). *J. Coast. Res.* **2024**, *113*, 748–752. [CrossRef]
53. Usai, A.; Simeone, S.; Trogu, D.; Porta, M.; De Muro, S. A morphometric analysis of embayed beaches: Southern Sardinia Island. *Geomorphology* **2025**, *483*, 109838. [CrossRef]
54. Vacchi, M.; De Falco, G.; Simeone, S.; Montefalcone, M.; Morri, C.; Ferrari, M.; Bianchi, C.N. Biogeomorphology of the Mediterranean *Posidonia oceanica* seagrass meadows. *Earth Surf. Process. Landf.* **2017**, *42*, 42–54. [CrossRef]
55. Trogu, D.; Buosi, C.; Ruju, A.; Porta, M.; Ibba, A.; De Muro, S. What happens to a Mediterranean microtidal wave-dominated beach during significant storm events? The morphological response of a natural Sardinian beach (Western Mediterranean). *J. Coast. Res.* **2020**, *95*, 695. [CrossRef]
56. Trogu, D.; Simeone, S.; Ruju, A.; Porta, M.; Ibba, A.; DeMuro, S. A four-year video monitoring analysis of the *Posidonia oceanica* banquette dynamic: A case study from an urban microtidal Mediterranean beach (Poetto Beach, Southern Sardinia, Italy). *J. Mar. Sci. Eng.* **2023**, *11*, 2376. [CrossRef]
57. Sardegna Geoportale. Data Download—Regione Sardegna. 2023. Available online: https://www.sardegnageoportale.it/accessoaidati/downloaddati/ (accessed on 12 July 2025).

58. De Falco, G.; Ferrari, S.; Cancemi, G.; Baroli, M. Relationship between sediment distribution and *Posidonia oceanica* seagrass. *Geo-Mar. Lett.* **2000**, *20*, 50–57. [CrossRef]
59. Marini, A.; Murru, M. Movimenti tettonici in Sardegna fra il Miocene superiore ed il Pleistocene: Tectonic movements in Sardinia between upper Miocene and Pleistocene. *Geog. Fis. Dinam. Quat.* **1983**, *6*, 39–42.
60. Biondo, M.; Buosi, C.; Trogu, D.; Mansfield, H.; Vacchi, M.; Ibba, A.; Porta, M.; Ruju, A.; De Muro, S. Natural vs. anthropic influence on the multidecadal shoreline changes of Mediterranean urban beaches: Lessons from the Gulf of Cagliari (Sardinia). *Water* **2020**, *12*, 3578. [CrossRef]
61. Carmignani, L.; Oggiano, G.; Barca, S.; Conti, P.; Salvadori, I.; Eltrudis, A.; Funedda, A.; Pasci, S. Geologia della Sardegna: Note illustrative della Carta geologica della Sardegna a scala 1:200,000. *Mem. Descr. Carta Geol. Ital.* **2001**, *60*, 1–283.
62. Funedda, A.; Oggiano, G. Outline of the Variscan basement of Sardinia. *Rend. Soc. Paleontol. Ital.* **2009**, *3*, 23–35.
63. Sardegna Geoportale. WMS Service (Autonomous Region of Sardinia). Available online: https://webgis.regione.sardegna.it/geoserverraster/ows?service=WMS&request=GetCapabilities (accessed on 27 April 2025).
64. Boak, E.H.; Turner, I.L. Shoreline definition and detection: A review. *Coast. Eng.* **2005**, *214*, 688–703. [CrossRef]
65. Thieler, E.R.; Himmelstoss, E.A.; Zichichi, J.L.; Ergul, A. The Digital Shoreline Analysis System (DSAS) Version 4.0—An ArcGIS extension for calculating shoreline change. In *U.S. Geological Survey Open-File Report*; No. 2008-1278; U.S. Geological Survey: Reston, VA, USA, 2009. [CrossRef]
66. Virdis, S.; Oggiano, G.; Disperati, L. A geomatics approach to multitemporal shoreline analysis in Western Mediterranean: The case of Platamona-Maritza Beach (Northwest Sardinia, Italy). *J. Coast. Res.* **2012**, *28*, 624–640.
67. Manca, E.; Pascucci, V.; Deluca, M.; Cossu, A.; Andreucci, S. Shoreline evolution related to coastal development of a managed beach in Alghero, Sardinia, Italy. *Ocean Coast. Manag.* **2013**, *85*, 65–76. [CrossRef]
68. Manno, G.; Lo Re, C.; Ciraolo, G. Uncertainties in shoreline position analysis: The role of run-up and tide in a gentle slope beach. *Ocean Sci.* **2017**, *13*, 661–671. [CrossRef]
69. Allan, J.C.; Komar, P.D.; Priest, G.R. Shoreline variability on the high-energy Oregon Coast and its usefulness in erosion-hazard assessments. *J. Coast Res.* **2003**, *19*, 106–115.
70. Rete Ondametrica Nazionale. ISPRA (Istituto Superiore per la Protezione e la Ricerca Ambientale). Available online: https://www.mareografico.it/it/stazioni.html (accessed on 27 April 2025).
71. Sardegna Geoportale. Download Raster (Autonomous Region of Sardinia). Available online: https://www.sardegnageoportale.it/webgis2/sardegnamappe/?map=download_raster (accessed on 24 April 2025).
72. Stockdon, H.F.; Holman, R.A.; Howd, P.A.; Sallenger, A.H., Jr. Empirical parameterization of setup, swash, and runup. *Coast. Eng.* **2006**, *53*, 573–588. [CrossRef]
73. Korres, G.; Ravdas, M.; Denaxa, D.; Sotiropoulou, M. Mediterranean Sea Waves Reanalysis. 2021. Available online: https://data.marine.copernicus.eu/product/MEDSEA_MULTIYEAR_WAV_006_012/description?view=-&option=-&product_id=- (accessed on 4 July 2025).
74. Nerves, A.; Rivera, F.D.; Blanco, A.; Tirol, Y.; Nadaoka, K. Shoreline change analysis in New Washington, Aklan using Digital Shoreline Analysis System (DSAS). *ISPRS Ann. Photogramm. Remote Sens. Spatial Inf. Sci.* **2024**, *10*, 111–117. [CrossRef]
75. Shafique, S.; Sarwar, F.; Kausar, S.; Abbas, S.; Khalid, M. Identification of shoreline changes using Digital Shoreline Analysis System (DSAS): A case study of Karachi Coast, Sindh, Pakistan. *Pak. J. Sci.* **2024**, *76*, 179–189. [CrossRef]
76. Akköprü, E.; Taş, M. Coastal geomorphology and coastal erosion of Phaselis Ancient City and its surroundings. *Phaselis* **2023**, *9*, 51–63. [CrossRef]
77. Gharnate, A.; Taouali, O.; Mhammdi, N. Shoreline change assessment of the Moroccan Atlantic coastline using DSAS techniques. *J. Coast. Res.* **2024**, *40*, 418–435. [CrossRef]
78. Dutta, D.; Kumar, T.; Jayaram, C.; Akram, W. Shoreline change analysis of Hooghly Estuary using multi-temporal Landsat data and Digital Shoreline Analysis System. In *Geographic Information Systems and Applications in Coastal Studies*; Zhang, Y., Cheng, Q., Eds.; IntechOpen: London, UK, 2022. [CrossRef]
79. Baig, M.R.I.; Ahmad, I.A.; Shahfahad; Tayyab, M.; Rahman, A. Analysis of shoreline changes in Vishakhapatnam coastal tract of Andhra Pradesh, India: An application of digital shoreline analysis system (DSAS). *Ann. GIS* **2020**, *26*, 361–376. [CrossRef]
80. Crawford, T.W.; Islam, M.S.; Rahman, M.K.; Paul, B.K.; Curtis, S.; Miah, M.G.; Islam, M.R. Coastal erosion and human perceptions of revetment protection in the lower Meghna Estuary of Bangladesh. *Remote Sens.* **2020**, *12*, 3108. [CrossRef]
81. Mathiesen, M.; Goda, Y.; Hawkes, P.J.; Mansard, E.; Martín, M.J.; Peltier, E.; Thompson, E.F.; Van Vledder, G. Recommended practice for extreme wave analysis. *J. Hydraul. Res.* **1994**, *32*, 803–814. [CrossRef]
82. Dolan, R.; Davis, R.E. Coastal Storm Hazards. In *Coastal Hazards: Perception, Susceptibility and Mitigation*; Finkl, C.W., Jr., Ed.; Journal of Coastal Research Special Issue (No. 12); Coastal Education & Research Foundation: Coconut Creek, FL, USA, 1994; pp. 103–114.
83. Karunarathna, H.; Pender, D.; Ranasinghe, R.; Short, A.D.; Reeve, D.E. The effects of storm clustering on beach profile variability. *Mar. Geol.* **2014**, *348*, 103–112. [CrossRef]

84. De Muro, S.; Porta, M.; Pusceddu, N.; Frongia, P.; Passarella, M.; Ruju, A.; Buosi, C.; Ibba, A. Geomorphological processes of a Mediterranean urbanized Beach (Sardinia, Gulf of Cagliari). *J. Maps* **2018**, *14*, 114–122. [CrossRef]
85. Ferrara, C.; Palmerini, V. Indagine sedimentologica sulla dinamica della linea di costa in facies sabbiosa nel settore centrale del Golfo di Cagliari. *Boll. Soc. Sarda Sci. Nat.* **1974**, *14*, 55–76.
86. Brambilla, W. Caratterizzazione Morfodinamica della Spiaggia del Poetto. Ph.D. Thesis, University of Cagliari, Cagliari, Italy, 2015.
87. Regione Autonoma della Sardegna. Piano di Gestione del Rischio di Alluvioni (PGRA): Secondo Ciclo di Pianificazione. Available online: https://pianogestionerischioalluvioni.regione.sardegna.it/index.php?xsl=2425&s=435566&v=2&c=95271&t=1&tb=14006 (accessed on 4 July 2025).
88. Carlini, D. Valutazione Preliminare delle Applicazioni Operative in Tema di Rimozione delle Biomasse sui Sistemi di Spiaggia della Sardegna: Analisi dei Dati R.A.S. per le Annualità 2018–2022. Bachelor's Thesis, University of Cagliari, Cagliari, Italy, 2024.